UNIVERSITAT POLITÈCNICA DE CATALUNYA
BARCELONATECH
Escola d'Enginyeria de Telecomunicació
i Aeroespacial de Castelldefels

TREBALL DE FI DE GRAU

TFG TITLE: Design and test of the bus of very small solar sail

DEGREE: Grau en Enginyeria d'Aeronavegació

AUTHORS: Víctor Navarro Juárez

ADVISOR: Jordi L. Gutierrez

SUPERVISOR: Jordi L. Gutierrez

DATE: October 28, 2017

Título: Diseño y test del bus de una vela solar muy pequeña

Autores: Víctor Navarro Juárez

Director: Jordi L. Gutierrez

Supervisor: Jordi L. Gutierrez

Fecha: October 28, 2017

Resumen

Con el avance en el campo de la tecnología, los sistemas aeroespaciales han ido evolucionando con el paso de los años. La tendencia de reducir el tamaño, peso y costes aumentado la eficiencia de los diferentes elementos ha abierto un amplio abanico de posibilidades. Así como antes la elaboración de cualquier vehículo espacial suponía unos costes económicos extremadamente altos dejando esta posibilidad solo a grandes compañías. Con la aparición de los conocidos nanosatélites hasta los femtosatélites esta posibilidad se ha abierto a pequeñas compañías o grupos universitarios de investigación, permitiendo a su vez, el avance científico en la exploración espacial.

En este proyecto se presenta el diseño del bus para una vela solar muy pequeña en el que se incluyen los sub-sistemas de potencia, comunicación y el ordenador de abordo así como la descripción de la misión. La principal dificultad de este proyecto viene reflejada en los requisitos de masa, limitando el peso máximo de todos los sub-sistemas mencionados anteriormente a 50 gramos.

Title : Design and test of the bus of very small solar sail

Authors: Víctor Navarro Juárez

Advisor: Jordi L. Gutierrez

Supervisor: Jordi L. Gutierrez

Date: October 28, 2017

Overview

With the advance on technology field, aerospace systems have been evolving during the last years. Tendency on reducing size, mass and cost by increasing the efficiency on different elements has opened a wide range of possibilities. Few years ago, the elaboration of any spacecraft involved high economical costs leaving this possibility only to big companies, with the appearance from nanosatellites to fentosatellites, this possibility has been open to small companies or university research groups, allowing at the same time, scientific advance on space exploration.
In this project is presented the design of the bus for a very small solar sail, which includes the electrical power subsystem, communication subsystem and the on-board computer. The main difficulty on this project resides on the mass requirements, limiting with a maximum weight of 50 grams for all those subsystems listed before.

Me gustaría dedicar este trabajo a mis padres y a mi hermano por haberme apoyado todo este tiempo. También, me gustaría agradecer todo el apoyo recibido tanto por parte de mis compañeros de proyecto: Carlos Díez y Carles Pié como de mi tutor: Jordi Gutiérrez.

Este proyecto no hubiese sido igual sin ninguno de vosotros.

CONTENTS

LIST OF FIGURES

LIST OF TABLES

LIST OF ACRONYMS

JAXA: Japan aerospace exploration agency.
NASA: National aeronautics and space administration.
MEMS: Microelectromechanical systems.
ADCS: Attitude determination and control subsystem.
EPS: Electric power subsystem.
BOL: Beginning of life.
EOL: End of life.
RCD: Reflective Control Device.
SPI: Serial Peripheral Interface.
I^{2}C: Inter-Integrated Circuit.
ADC: Analog-to-digital converter.
L2: Lagrangian point 2.
R$_E$ Earth Radii.
IMU: Inertial measurement unit.
LEO: Low Earth orbit.
LSb: Less significant bit.
EEPROM: Electrically erasable programmable read-only memory.
SRAM: Static random access memory.
USART: Universal Synchronous and Asynchronous Receiver-Transmitter.
VSWR: Voltage standing wave ratio.
I/O: Input / Output.
PWM: Pulse-width modulation.

GENERAL INTRODUCCTION

Propulsion devices are one of the most restrictive subsystems in small satellites, many of them even showing a complete lack of them. In this set of three Final Degree Thesis, we have explored the possibility of using a small solar sail to propel a femtosatellite.

As solar sails employ solar radiation pressure, do not carry any kind of hazardous materials (as would happen in most of the rest of propulsion systems), and therefore would have no constraints to be launched as a secondary payload.

Solar sails have been known to be feasible for a long time, but practical implementation was precluded until recently due to its difficult construction and deployment. As they use the pressure exerted by solar light, solar sails do not require to carry any kind of fuel and, as long as they remain illuminated by the Sun, they can propel themselves for an indefinitely long time.

The first solar sails were IKAROS, launched by JAXA in 2010, and Nanosail-D, launched by NASA in 2011. In both cases, the missions were a complete success. IKAROS is especially relevant in this regard because its mission took it to the orbit of Venus, thus probing not only that the propulsion mechanism was physically sound, but also technologically feasible. Several solar sails projects are currently underway; the most salient is Lightsail-2, developed by The Planetary Society.

Its main strength is also its most important weakness: by using the tiny force exerted by light pressure, their fabric must be extremely light, and thus require a very flimsy material. Even in our case, with a very small sail of just 10 m^2, it is impossible to launch the sail deployed. Hence, a mechanism to fold it on the ground, and allow an easy and unsupervised unfolding once in space, must be devised. The fabric composing the sail must also be protected against rips and deep wrinkles, something quite difficult with such a delicate material.

The payload for our sail, that we have christened FemtoSail, will accordingly be very low-mass. The bus of the active part of the FemtoSail will have a mass under 50 grams. Our goal is to have as high an acceleration as possible and obviously this calls for a very small total mass. The total mass of the sail will be, at most, 100 grams.

FemtoSail will be folded and carried into orbit inside a canister with the same form factor as a 3U CubeSats (then, a rectangular prism with a base 10 cm in side, and a long side of 30 cm). Once in orbit, the canister will open a hatch and the sail will be ejected. After the ejection, the solar sail must unfold by itself.

The general layout is as follows: the sail will be square in shape, and the bus will be composed of an on board computer, a battery that will store the energy gathered by solar cells, a flat antenna and transmitter, and electrochromic systems to allow attitude control. As the energy gathered by the solar cells would be quite reduced, communications would be of the burst kind.

The mission for such a small spacecraft must be compatible with its capabilities, that due to its very low mass are rather limited. It is equally important to consider in which regards a set of femtosatellites would provide an advantage as compared to standard satellites. A sensible option is to have a large number of femtosatellites to carry out a determination of some property in multiple points. As an example, we will focus on their use as probes of

the Earth's magnetotail. Magnetospheric physics has been one of the main focus of Space Science since the very beginning of Human exploration of the environments of the Earth. However, the number of satellites involved in this kind of investigations has always been quite small, and usually restricted to Low Earth Orbit. Our mission would determine the magnetic field strength and some plasma properties simultaneously in several points.

Using a solar sail with manoeuvring capabilities would constitute a valuable asset, as it would be possible to make several scans or particular zones of the magnetosphere without waiting for the orbital motion allow for a new pass through the region of interest.

The magnetosphere is a very dynamic region, with multiple physical phenomena deploying simultaneously, and its study is very involved. Having good quality data in many different (albeit nearby) points would allow a deeper understanding of the processes going on.

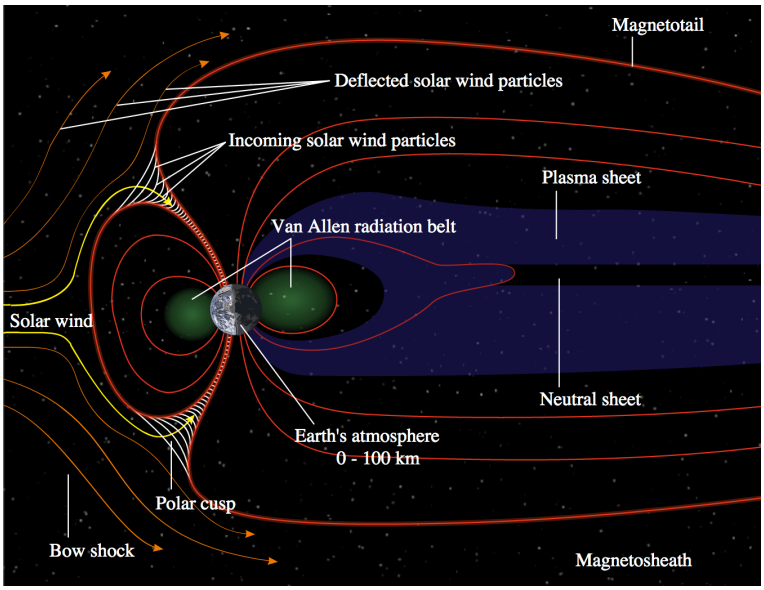

Figure 1: Schematics of the magnetosphere of the Earth and its interaction with the solar wind. The magnetotail is the region in purple to the right of the Earth.

The magnetotail is an ill-known part of the magnetosphere, observed basically in the Lunar environment, both from orbit as well as from the surface. However, the dynamics and properties of the magnetic field of the Earth beyond the Moon orbit is uncharted waters.

The solar wind stretches out the terrestrial magnetic field into an elongated and dynamic structure. Just a few missions have observed this region, the most remarkable ones are ISEE-3 (International Sun-Earth Explorer 3), and Geotail. Both were able to observe the magnetotail up to a distance of 200–220 Earth radii, finding that the plasma sheet is still well-defined at these distances.

The magnetotail is composed of two lobes, one above the other below the equatorial plane, where the magnetic field lines are almost parallel. Here the plasma density is low, and at large distances from the Earth, they are penetrated by the solar wind. Eventually, the weakening magnetic field of the Earth becomes attached to the interplanetary magnetic field, allowing the plasma in the lobes to escape.

Between the lobes there is a region on weak magnetic field and relatively high plasma density, the plasma sheet. Its width ranges from 2 to 6 Earth radii, and it also extends

to very long distances (around 200 Earth radii). As the magnetic field here is weak, the plasma moves more freely than in the case of the lobes. There is a cross tail current flowing across the plasma sheet in the dawn-dusk sense; this electrical current is responsible of generating the local magnetic field. Two currents, flowing through the magnetopause on the north and south lobes, close the circuit. The central part of this region is almost neutral, and is called the neutral sheet.

As the plasma sheet is continuously loosing plasma to the interplanetary medium, it is necessary some replenishment mechanism. While there are several hypotheses, the actual mechanism remains difficult to explain. A set of simultaneous measurements in multiple locations could greatly help to ascertain its nature.

The goal of this work is to provide a very basic, low-cost system to provide in-situ measurements of the magnetic field in this region. One very basic difficulty for a classical satellite would be the scarcity of missions allowing a secondary payload launch. In the case of solar sails, the initial orbit is not that important, as their propulsive capabilities allow them to navigate to achieve the final orbit (even if the time required to do so can be substantial).

As will be described further on, the envisioned mission carries a MEMS magnetometer to determine the magnetic field in different location of the magnetotail, near its neutral sheet.

This thesis work is a part of a series of three Final Degree Thesis simultaneously carried on to generate a full pre-A phase description. Then, the introduction up to this point is shared with the other two Degree Thesis (titled *Guidance, Navigation and control of a very small solar sail* and *Design, deployment mechanism, and thermal control of a very small solar sail*).

In this part, we propose to design the bus (including power, on board computer, and telecommunications, but excluding attitude control) of a solar sail with a total surface of 10 square metres.

The maximum mass of the electronics system must be under 50 grams, as the total mass of the solar sail (thus including bus, payload and the fabric) must be under 100 grams.

The electronic design must be able to fulfill all the necessary tasks to support the payload, as well as the ADCS system.

INTRODUCCTION

The difference between a solar sail and typical femtosatellite resides on the propulsion subsystem, the nature of this subsystems offers infinite thrust in time but requires lot of surface. At the same time, the deployment is specially one of the most critical phases for solar sail inasmuch as the folding of big a surface on the small volume of 3U cubesat entails big problems.

In this project will be discussed the design of the electronic conforming very small solar sail which must fulfil all the necessary tasks to support the payload, as well as the ADCS system. Unlike the above, the electronic design of a solar sail is quite similar to typical femtosatellite, with the mass restrictions that it supposes. It is therefore, that the main difficulty on this project resides on attempt to reduce the mass by keeping the efficiency of the electronic devices as much as possible.

Mission consists on circular orbit whit focus on Lagrangian point L2 on the system Sun-Earth. The objective of this orbit is to take advantage of the geometry of L2 which is located at the night side of the Earth to measure the magnetic field of the magnetotail with the help of one magnetometer which will be the only payload of the system.

All the data related with magnetic field has to be sent to the Earth by the communication subsystem. Values on magnetic field must be accompanied with position, to establish a magnetic field chart, and orientation, since the sensor measures on three axis. As communication is the most power hungry subsystem for most femtosatellites and solar cells can not provide enough energy, the duty cycle has to be reduced by introducing the burst communication technique.

Related with EPS, the only viable possibility to generate energy is by using photovoltaic cells, this involves directly a contradiction with the basis of the solar sailing as the propulsion subsystem needs materials with a high index of reflectivity to take the maximum advantage of photons lineal moment. Meanwhile solar cells, by definition, haves low reflectivity values in order to use the maximum solar radiation. Thus, solar cells must be as small as possible to not hinder solar sail behaviour. To get conservative dimensionalization for the solar cells, it have been taken into account the EOL power generation supposing always a worst case scenario of illumination angle of 30° to ensure electrical energy for all phases of the mission.

All subsystems have to been interconnected to on-board computer to know how and when to act. The assignment for the on-board computer is to establish a relationship between the inputs from the sensors (gyroscopes, accelerometers, battery state...) with the outputs which are the transceiver, the actuators (RCDs) and a set of protection switches. This system have to order when the solar sail needs to charge battery, when it is necessary to start burst communications and how RCDs have to behave. To decide this operations, OBC have to read data from the sensors through SPI and I^2C communication protocols as well as the analogical inputs which must be converted to digital signal through ADC.

The maximum mass of the electronic system must be under 50 grams. Requirement that has forced to find always the most efficient way to design the solar sail.

CHAPTER 1. MISSION DESIGN, OBJECTIVES AND MOTIVATIONS

1.1. Mission description

Usage of solar sailing as an alternartive of other conventional spacecraft propulsion systems provides a huge number of creative solutions which can allow advances on scientific research. Using the solar pressure as the only propulsion system results on a time-infinite thrust which allows the spacecraft to orbit indefinitely on non-Keplerian orbits. Futhermore, the ultra light-weight satellite makes the deployment simplest and, therefore, cheapest than other conventional spacecrafts. On the minus side, the slightness of solar pressure make for just the tiniets acceleration, always clearly below 1 mm/s^2.

The easy deployment and low-cost of this relatively new technology creates a perfect combination to the study on many scientific fields that could not be undertaken some years ago, specially those that could require of a large number of simulatenous measurements in different locations, as well as those testing risky hypotheesis. The focus of this project is the study of the Earth Magnetotail. As it was previously mentioned, the limitation of the conventional spacecraft's has prevented the study of the magnetic field among the Lagrangian point L2 of the Earth-Sun system.

The orbit envisioned for the project is a zero-inclination, circular orbit with the center on the Lagrangian point L2 (located at $\sim$1 500 000 km from the Earth in the opposite direction of the Sun), using it as artificial celestial body due to the characteristics discussed on the section (1.3). The payload on board is a magnetometer measuring the magnetic field in each point of the orbit with 1Hz sampling rate. The goal of the mission is to send the data related with magnetic field on the magnetotail to the Earth.

On the following sections, we will describe the nature of the Magnetotail as well as the definition of Lagrangian points and on-board sensors used.

1.2. Magnetotail

The Earth can be understood as a huge magnet which has his own magnetic field. Due to the interaction with the solar wind, this magnetic field is deformed resulting on a shape compressed on the sun direction and and expanded on the other side. The strength of this magnetic field has been the focus of many studies about the Earth surface and it is a really useful tool on different positioning instruments. Moreover, on LEO orbits, this magnetic field can be used on the attitude and determination subsystem.

The first theoretically introduction of Magnetotail phenomena was described by *J.H. Piddington* on 1960, on study about the geomagnetic storms. Study where was predicted the deformation of the terrestrial magnetic field by the solar wind. But, at that time, solar wind were not understood as continuous plasma flux so such magnetic field was thought as a temporally distribution. On the same year, *F.S. Jhonson* considers the effect of a continuous fast moving solar plasma, which could deform the magnetic field in a tear shape with a front to back radio from 1 to 6. Four years later, at 1964, *A.J. Dessler* concluded that the

minimum length of the magnetotail would be at least 100 R_E (637 810 km).

Years later, on August 1978, ISEE3 was launched to study the magnetotail effect between 60 and 240 R_E by describing a very particular orbit. Originally, ISEE3 was stationed in orbit about the sunward liberation point L1, located 240 R_E from the earth towards the sun to study the interaction of the solar wind with the earth's magnetic field and dynamic processes within the magnetosphere. In June 1982 propulsion system redirects ISEE3 in to a series of looping trajectories through the earth's tail by using lunar swingbys, achieving the apogee on February 1993 of 221 R_E.

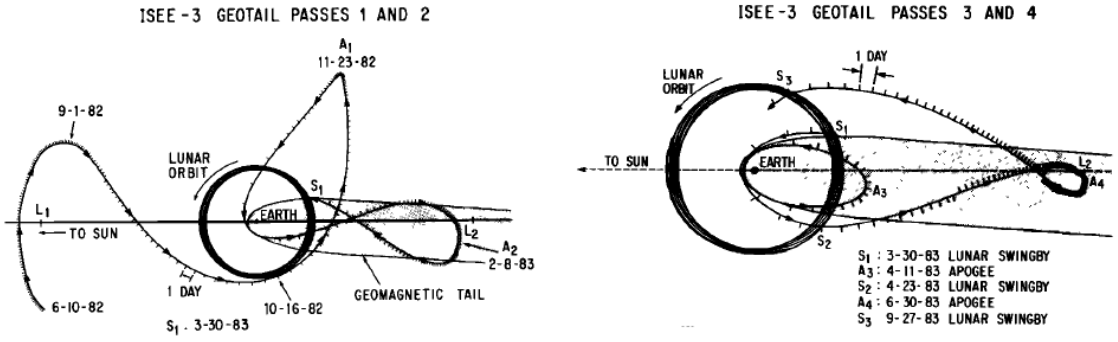

Figure 1.1: The orbit described by ISEE3 projected onto ecliptic plane from liberation point L_1. Source: ISEE-3 distant geotail results, *Bruce T. Tsurutani* & *Tycho T. yon Rosenvinge*.

The results obtained by ISEE3 were really useful to the comprehension of the magnetotail at distant points. A sample of the magnetic field obtained from ISEE3 at GSM coordinates X = -77.7 R_E, Y = + 12.0 R_E, and Z = +4.6 R_E is shown on the figure below.

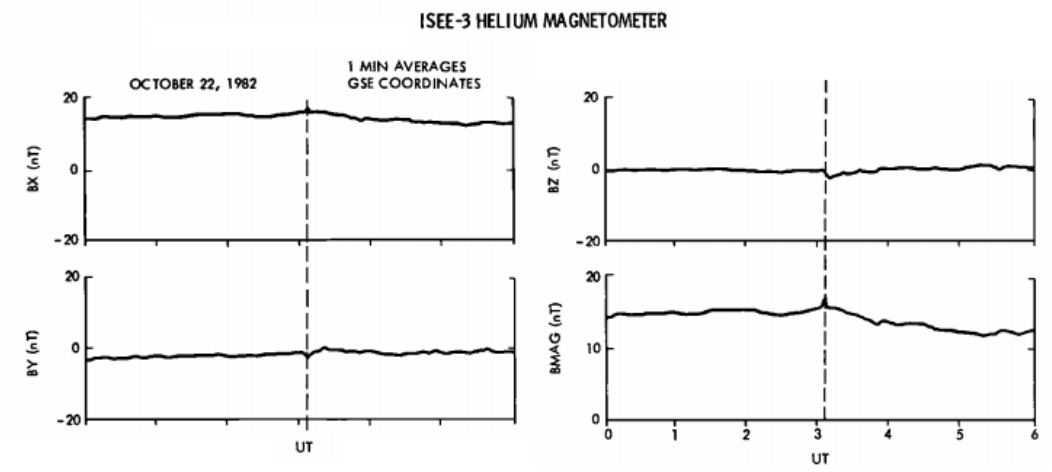

Figure 1.2: Six hours of ISEE-3 magnetic lobe observations are displayed in GSM coordinates. Source: ISEE3 Geotal observations. *Geophysical Research Letter*s.

1.3. Lagrangian points

On classical orbits, where only two bodies are involved in the orbital motion and dynamics, it is easy to compute the behaviour of both of them. For example, the acceleration of a satellite orbiting around the Earth only depends on the Earth gravitational force; thus, by using the second Newton's Law, and recalling that the only force involved is, as said before, Earth's gravity, it s a simple matter to determine that the acceleration is

$$F = m \cdot \ddot{x} \rightarrow \ddot{x} = \frac{G \cdot M_E \cdot \cancel{m_{sat}}}{x^2 \cdot \cancel{m_{sat}}} \tag{1.1}$$

Understanding x as a two dimensional vector giving the distance between the two bodies, the acceleration takes vector form by modifying (1.1) to:

$$\ddot{x} = \frac{G \cdot M_E \cdot (x_1 - x_2)}{|x_1 - x_2|^3} \tag{1.2}$$

Lagrangian points appear when considering the restricted three-body problem. The addition of a third body to the system generates a perturbation on the gravity forces experimented on the satellite, changing in this way, the orbital velocity. It is also necessary to take into account that the reference system of the satellite is non-inertial, and then it is mandatory to consider the centrifugal force.

Expressing again the Newton's second principle by adding the third body, it is possible to study the velocity of the satellite by permuting between the three bodies as:

$$\ddot{x}_i = -G m_j \frac{x_i - x_j}{|x_i - x_j|^3} - G m_k \frac{x_i - x_k}{|x_i - x_k|^3} \tag{1.3}$$

The equation above (1.3) describes the velocity of the third body (which would be the satellite) as a function of the gravity from the other two bodies, which in the case of interest for this work would be the Earth and the Sun. The sub-index i, j and k are used because there exists analogous equations for the other two bodies which could be found by doing the two ordered permutations [(1,2,3), (2,1,3) and (3,1,2)].

Those three second order vector differential equations studied on the centre of masses of one body, the satellite for example, gives 6 constraints which are:

$$\sum_{i=1}^{i=3} m_i x_i = 0 \qquad and, \qquad \sum_{i=1}^{i=3} m_i \ddot{x}_i = 0 \tag{1.4}$$

In February 1971, *R. Broucke* and *H. Lass* on "A note on relative motion in the general three-body system" found that the expression before can be written on a very symmetric form when one considers the relative positions of the bodies as: $s_i = x_j - x_k$.

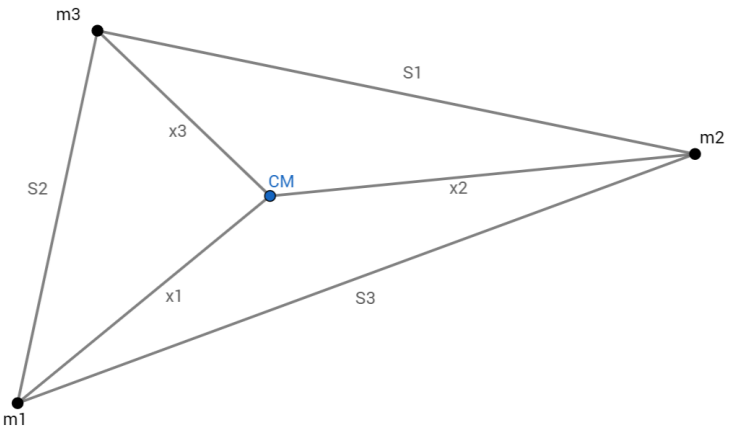

Figure 1.3: Position of the vectors and their relative position on the three body problem representation.

Being,

$$s_1 + s_2 + s_3 = (x_2 - x_3) + (x_1 - x_3) + (x_1 - x_2) = 0$$

By expressing (1.3) in terms of relative position:

$$s_i = -GM\frac{s_i}{s_i^3} + m_i\Gamma \tag{1.5}$$

$$where, \quad M = m_1 + m_2 + m_3 \quad and \quad \Gamma = \sum_{i=1}^{i=3}\frac{s_i}{s_i^3} \tag{1.6}$$

The solution for these differential equations are chaotic and cannot be solved in closed form. But Joseph Louis Lagrange obtained the analytical solution for the restricted problem, in which one body is much lighter than the other two (a very close approximation for the study of an spacecraft and two massive celestial objects).

The equation for restricted problem has finally 5 analytical solutions. These five locations are known as Lagrangian points, and represent the positions on the ecliptical 3 body plane where the net forces result in equilibrium configurations. These analytical solutions are:

$$L_1 = \left(R\left[1 - \left(\frac{\alpha}{3}\right)^{1/3}\right], = 0\right) \qquad L_4 = \left(\frac{R}{2}\left(\frac{M_1 - M_2}{M_1 + M_2}\right), \frac{\sqrt{3}}{2}R\right)$$

$$L_2 = \left(R\left[1 + \left(\frac{\alpha}{3}\right)^{1/3}\right], = 0\right) \qquad L_5 = \left(\frac{R}{2}\left(\frac{M_1 - M_2}{M_1 + M_2}\right), -\frac{\sqrt{3}}{2}R\right)$$

$$L_3 = \left(-R\left[1 + \frac{5\alpha}{12}\right], = 0\right) \qquad Where, \alpha = \frac{M_2}{M_1 + M_2}$$

Graphical representation of those points:

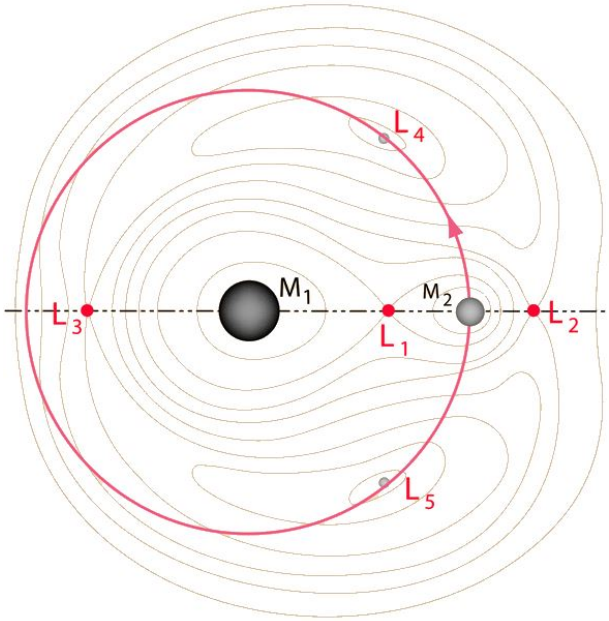

Figure 1.4: Lagrange points graphical representation.

An easier way to understand Lagrangian points without mathematical and physical development is by understanding the gravitational effects on those points. For example (referencing on figure 1.4), satellite situated at L1 must orbit faster if only considers M_1 than the same satellite located on M_2 position or anywhere farthest. But, by adding M_2 gravitational force, M_2 will attract satellite by reducing the total net force exerted by M_1 and, therefore, the spacecraft needs less speed to maintain its orbit, so it can slow down. Exactly at L1 point, satellite is totally quiet on the reference frame. This reasoning could be applied for any of the 5 Lagrangian points.

1.4. Payload

As the objective of the mission is to do more detailed study and find more information about the Magnetotail, the solar sail will need at least one magnetometer in order to measure the magnetic field. In addition, with the determination and attitude system it will be possible to determine the space coordinates in order to create a chart based on the magnetic field per space position.

Then, it is the goal of this section select the sensor that will be the only payload of the solar sail. For this, we got the restrictions on power consumption, data rate for the communications and physical weight. As the objective of the mission is to know more accurately the intensity on the magnetic field it is not possible to establish exactly the range and the resolution of magnetometer, so it should be approximated.

Magnetometers are hugely used on space applications for the attitude and determination systems using the magnetic field as a reference mainly on LEO. Therefore, there are a considerably different types of magnetometers on space applications.

To select a model with specific characteristics it must be known the ranges that it will be exposed on orbit. The Earth's surface magnetic fields ranges varies between $\pm$0.25 and $\pm$0.65G. As the magnetic field intensity decay with the distance, at any orbit around the Earth should be, theoretically under those limit. It is true that the presence of the solar wind creating the magnetotail concentrate charged particles on the night-side of the Earth making the magnetic field to not fall as in free space conditions. Is therefore, fixed as a minimum range, by leaving wide security margin, to $\pm$0.65G. Fortunately, the range for most magnetometers used on space applications have ranges much higher and, therefore, range of measurements will not be much problem on magnetometer selection.

The magnetometer selected for being the only payload on board is the digital magnetometer LIS3MDL manufactured by STMicroelectronics. The selection of this device is due to their ultra low weight and by the capacity of gain sensitivity by reducing the dynamic range from $\pm$16 to $\pm$ 4 Gauss, obtaining higher resolutions with the 16 bit ADC. Other reasons are the voltage supply, which matches perfectly with the 3.3V for the main load and the low current consumption, reducing at the same time EPS size.

Specification	**LIS3MDL**		**Units**
	Min	Max	
Range	$\pm$ 4	$\pm$ 16	Gauss
Sensitivity	1711	6842	LSb/Gauss
Digital resolution	0.14	0.58	mGauss
ADC bit	16		bit
Output data rate	0.625	80	Hz
Voltage supply	1.9	3.6	V
Current	100		μA
Operating temperature	-40	85	$^{\circ}C$
Weight	0.018		grams
Size	2x2x1		mm

Table 1.1: Magnetometer LIS3MDL technical specifications (All provided on official datasheet).

Sensitivity is the minimum input signal required to produce specified output. In this case, it is expressed as Less Significant bit per Gauss (LSb/Gauss). This only means that there are needed 230 to 1370 bit position to measure 1 Gauss. In other words, the difference between two adjacent bits are for: 1711^{-1} = 0.56 mGauss to 6842^{-1} = 0.14 mGauss.

Datasheet of the magnetometer is annexed at the end of the document.

CHAPTER 2. ELECTRICAL POWER SUBSYSTEM

2.1. Introduction

The Electrical Power Subsystem, referred to as EPS below, has as objective to generate, store, distribute and control the electric energy of all spacecraft. In this chapter, we will analyse the mechanism in which energy will be generated, the amount of energy in relation with the needed mass, the dimensionalization of the elements used as storage, and the distribution system.

2.2. Energy generation

In some short term missions there is not needed for generation of energy due to the fact that the energy stored on a primary battery is enough for the whole mission. In our case, the mission will be operative for one year, then it is a mandatory to provide energy to the other subsystems.

There are different ways to generate energy as a function of the mission and spacecraft characteristics. They can be classified on three broad groups: static, dynamic and photovoltaic. Both, first and second groups are based on the use of a heat source to generate energy. The first one, static group receives his name due to the fact that it does not need any mobile part to generate energy. This group can be further split into two different types known as Thermionic and Thermoelectric. First one uses the temperature differences that can be generated between two metallic plates to generate an electron movement from cold plate to the hot one, thus generating a potential difference that can be used to directly charge a battery.

On the other hand, the generation of thermoelectric generation is based on the Seebeck effect, which describes the direct conversion of a temperature difference into electrical energy. This conversion is produced when two different metals are joined at the ends whit a temperature difference between them.

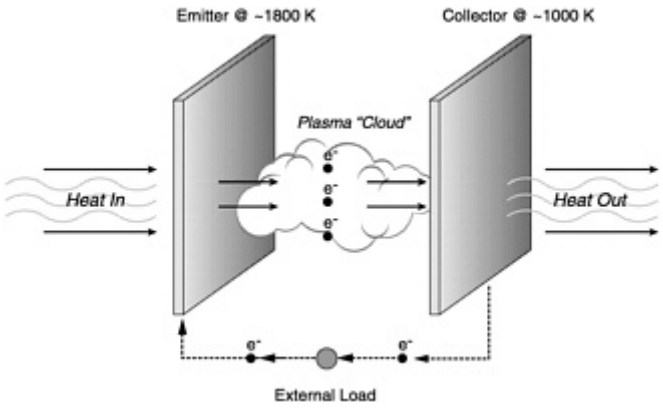

Figure 2.1: Basic thermionic converter schematic.

The generation of dynamic energy also uses temperature differences applying one of the three possible thermodynamics cycles (*Rankine, Brayton and Stirling*) to generate electric current but, this time, the system has mobile parts. All of them are based on a heat source to evaporate at high pressure some fluid; this hot vapour will make a turbine to spin and generate electrical energy. This heat source can be solar, or nuclear using radioisotope disintegration.

Last of three group is photoelectric energy. This is used on almost every spacecraft due to the fact that can generate passively energy with the only source of the solar radiation.

The generation of energy for this mission is severely limited mainly by the available mass. Taking into account the objectives of this project, we can see that the total mass of the bus can not exceed 100 grams, discarding all the possibilities of implementing any type of static and dynamic energy system due to the mechanical complexity (as well as high mass) of those systems. Leading on the conclusion that the only viable power sources are photovoltaic. On this project the photovoltaic energy is the one selected for many reasons: it is the best known and has better performances per unit mass.

2.2.1. Key parameters

To understand the type of photovoltaic system that will be used it is necessary to know the different existing types and their characteristics: configurations, design advantages and disadvantages, sizes, masses, etc.

The key parameters to identify the best system for a particular mission are: power peak, nominal power, operational temperature of solar cells, eclipse time, environment radiation, inclination to the normal vector between sun and spacecraft, on orbit life (Beginning of Life, BOL, and End of Life, EOL), mass and area.

Typically, solar cell performances are represented graphically by plotting the intensity versus voltage. With these plots, known as I-V plot, the user can easily identify different parameters for the solar cell as:

- Short-circuit current ($voltage = 0$): I_{SC}
- Open circuit voltage ($intensity = 0$): V_{SC}
- Maximum efficiency point (where the product I $\times$ V is maximum): J_{MP} = I_{MP} x V_{MP}

Typically, the short-circuit current (I_{SC}) is expresed as a function of area. For this reason, the intensity is represented with current density (J) units: $[A/m^2]$ (where A is for Ampere and not area). The usage of this units is due to the fact that the intensity, unlike the voltage, is proportional to the illuminated solar cell area. That is, an increase of the illuminated solar cell area implies a directly proportional increase on the generated current, but not on the voltage, which only depends on the material bandgap (see subsection 2.3).

For the solar cells sizing it is also necessary to take into account different factors which can negatively affect to the I-V curve. On this project we have studied the main reasons of solar cell efficiency deterioration: Operative temperature, environment radiation, illumination angle and eclipse duration.

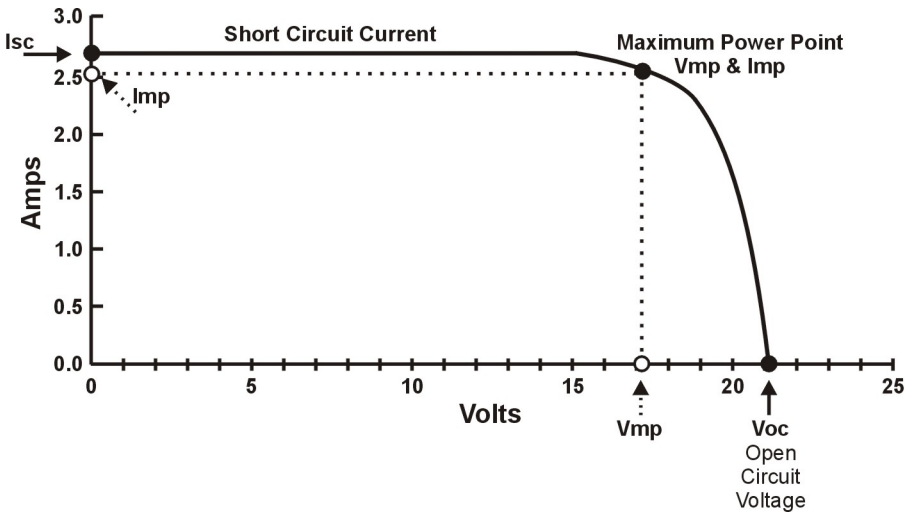

Figure 2.2: Typical I-V plot for solar cell.

Those reductions on efficiency are represented on different ways on the I-V plot as:

- Downwards translation on intensity axis.
- Translation toward the left on voltage axis.
- More pronounced rounding at the maximum power point

On all three scenarios, there is implicit a reduction on maximum power generation, and so it will be necessary to study the specific degradations for every type of solar cell on our EPS.

2.2.2. Differences between materials

The electrical current, or the current density generated by the solar cell is a function of illuminated area and has no relation with the material. On the other hand, the voltage generated is directly function of the material and, more exactly, the bandgap of it.

Every element has two states known as *Valence band* and *Conduction band*. The former makes reference to the insulating behavior of the material, while the latter one is related to the conducting state. The electrons are in valence or conduction band depending on its energy and the bandgap. Semiconductor materials are those which have a small, less than 3 eV, bandgap.

Photoelectric effect is due to the interaction between a photon which transfers part of its energy to an electron in the valence band in such a way that it moves to the conduction band. Thus, on an ideal case, the kinetic energy of the resulting electron will be equal to the energy of the incident photon minus the binding energy of the electron to the original atom.

By applying this theory to a real system we can find different types of inefficiencies. Firstly, just being over 0 kelvin changes the behavior of the materials conforming the solar cell, changing the values of the bandgaps and therefore, affecting negatively the efficiency.

Moreover, the solar cell can be studied as a black body with certain temperature, whereby it emits electromagnetic radiation that can be converted into heat, and transported by conduction. This effect is quantified on the following subsection (2.5.2 Temperature losses).

On the other hand, when a photon with an energy greater than the bandgap reaches a solar cell atom creates an electron - hole pair, which cand be converted into a current. But, if the energy of this photon is much larger than the bandgap, the excess energy is dissipated as heat affecting to the solar cell efficiency.

2.2.3. Triple junction GaP/GaAs/Ge

Most of the solar cells manufactured nowadays for terrestrial applications consist on single junction cells. The fact of only having one material implies that cell can not use all the solar radiation (2.3), but just a fraction of it. This systematically reduces the efficiency of the single junction solar cell, currently giving on high-quality solar cells efficiency values with a maximum of 20%.

To increment the efficiency, it is necessary to use a larger fraction of the electromagnetic radiation. This goal can be achieved by simultaneously using different materials with different bandgaps. Then, by adding more layers (more p-n junctions) with different bandgaps, the percentage of radiated energy used is larger and the cell becomes more efficient. According to a study by Green, M.A on 2003 (Third Generation Photovoltaics: Advanced Solar Energy Conversion) the theorical limits on solar cell efficiency, studied by William Shockley and Hans-Joachim Queisser, varies directly with the number of layers as:

Number of layers	Theoretical maximum efficiency (%)
1	40.8
2	55.5
3	63.2
4	67.9
∞	86.8

Table 2.1: Theoretic maximum efficiency as a function of p-n junction layers for photoelectric cells.

It is also needed to take into account that the number of layers causes an increase of the mass of the system and intrinsically adds more complexity to the fabrication and, therefore, to the cost of the solar cell. In addition, this increment on the efficiency is not linear: the difference between one and two layers implies an 14.7% of efficiency increase, while for the third and fourth only represents a 4.7%. Typically on aerospace industry the most used is triple junction cells because are the ones that adjust better this balance between efficiency and complexity, and have a larger power per unit mass ratio.

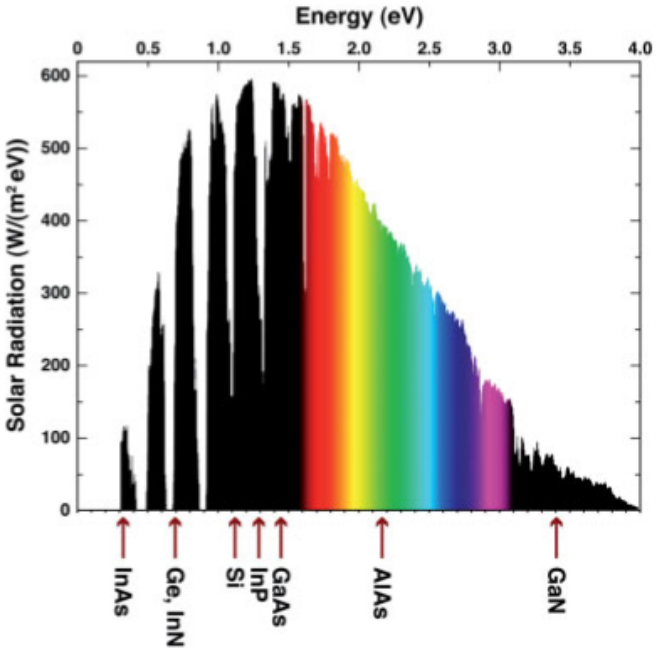

Figure 2.3: Solar radiation spectrum as a function of energy radiated (eV).

As we can see on figure 2.3, the sun radiation has a wide spectrum between 0.3 to 4 eV distributed in a similar way to a black-body distribution centred on, approximately, 1.4 eV. Whatsoever, to use the maximum possible spectrum with three different bandgaps, one of them needs to have a value close to 1.4 eV, with another one below this figure, between 0.3 and 1.4 eV, and one above, between 1.4 and 4 eV.

A set of elements that meet those properties (on ascending bandgap order) are: Germanium (Ge), Gallium arsenide (GaAs) y Gallium phosphide (GaP). With 2.26, 1.43 y 0.67 eV, respectively.

Joining the information of the table 2.1 with figure 2.3, the serial configuration of those elements (GaP/GaAs/Ge) makes possible the increment of the maximum theoretical efficiency from 40.8 to 63.2% leaving nowadays existing Triple Junction cells with efficiencies over 30%.

This maximum efficiency is obtained by using tandem configuration with the top cell responding on the short wavelengths (energies greater than 1.4 eV) and letting pass the long wavelengths through the bottom layers (see figure 2.4).

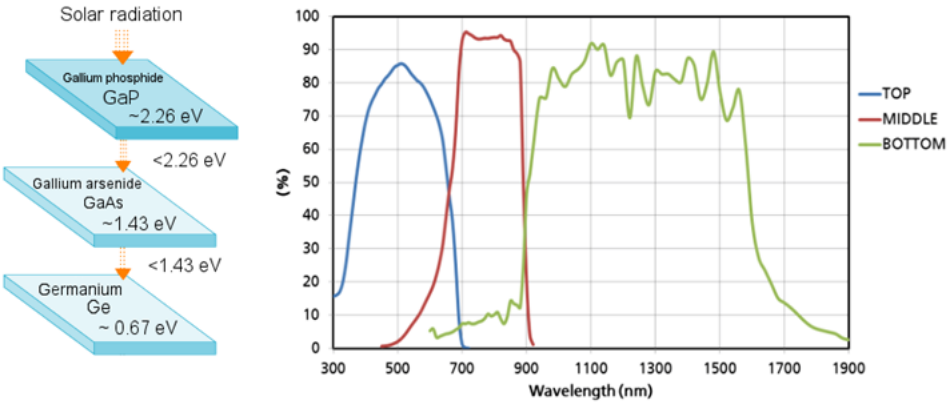

Figure 2.4: At the left: graphic representation of GaP/GaAs/Ge solar cell. At the right: portion of absorbed solar radiation spectrum (Source: CESI triple junction cell CTJ30 datasheet).

2.2.4. Dimensioning of the power subsystem

2.2.4.1. Generated energy at optimal conditions

This section and the following ones make reference to the annexes A, B and C. Attached at the end of the document, those annexes are the datasheets of three solar cells form different manufactures: Spectrolab, Azurspace and SolAero. This three have been chosen for being space qualified and offer the best performace on power per mass unit and power per area unit. Inside each manufacturer we have chosen the best quality solar cells as long as they are actually on production. Furthermore, SolAero is working on new high efficiency solar cell of 32.0%, but nowadays this cell is not on commertial production and it will not be included on the study of this project.

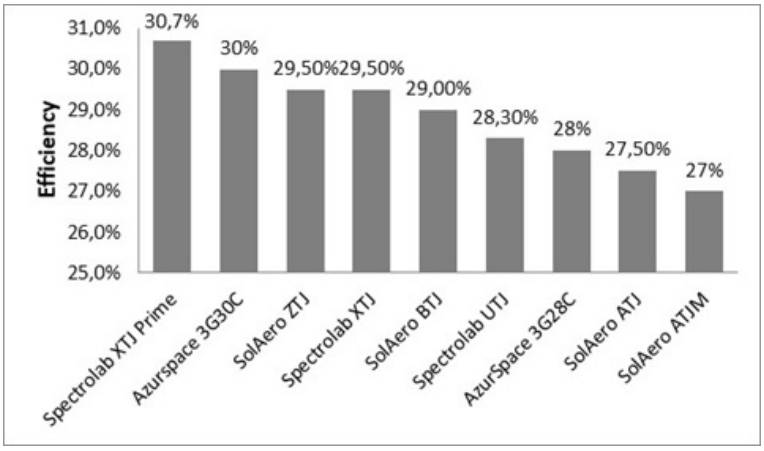

Figure 2.5: Efficiencies comparation for different Triple Junction solar cell from Spectrolab, AzurSpace and SolAero.

The maximum electrical power which offers a solar cell is defined by the I-V plot as the point where the product of those two magnitudes is maximum (the so-called knee of the plot). On this point those magnitudes are known as: V_{MP} and I_{MP}. Then, the maximum power that can be generated by the solar cell is:

$$P_{\mathrm{MAX}}[W] = I_{\mathrm{MP}} \times V_{\mathrm{MP}} \tag{2.1}$$

More accurately, it is necessary to use the intensity current expression and let the power as a function of illuminated area,

$$P_{MAX}[W/cm^2] = J_{\mathrm{MP}} \times V_{\mathrm{MP}} \tag{2.2}$$

Using datasheets annexed (A, B and C) to this document and applying this first approximation (2.2), we can determine the generated power for the Spectrolab, AzurSpace and SolAero cells:

Solar Cell	Power per unit area $[W/cm^2]$
Spectrolab	0.041586
AzurSpace	0.040312
SolAero	0.039765

Table 2.2: Solar cell's generated power per unit area.

Due to the absence of current density value for AzurSpace solar cell on its datasheet, it has been approximated as the "*current at max. power*" at BOL $(504.4mA)$ divided by the solar cell area $(30.18cm^2)$, resulting on: $0.01671W/cm^2$.

2.2.4.2. Temperature losses

There is an empiric relation, made by the physicist and astrophysicist *Y. P. Varshni*, between bandgap (E_g) and temperature (T) for semiconductor elements that can be expressed as:

$$E_G = E_0 - \frac{\alpha T^2}{T + \beta} \tag{2.3}$$

Where E_0 is the bandgap at 0 K and α and β are constants which depend on the specific material used. This equation represents experimental data for some semiconductors including GaAs and Ge. This variation on bandgap reduces the voltage generated.

At the same time, heating the solar cells will produce an increase on electron excitation, thus making easier to photons to make them free and increasing the amount of free electron - holes produced. This entails a current increase. At the same time, this extra temperature produces a concomitant increase in resistivity of the material.

As the voltage decrease faster than the intensity, the product of those two values has tendency to go down. Then, an increase on temperature implies a reduction on solar cell efficiency.

For this reason, the equation (2.2) should be modified by adding the temperature coefficients (facilitated on the annexed datasheets) which express the variation on the voltage and current density ($\triangle V_{\mathrm{MP}}$ and $\triangle J_{\mathrm{MP}}$, respectively) as a function of temperature. The modified equation reads,

$$P[\mathrm{W/cm^2}] = \mathrm{J_{MP}} + [\triangle \mathrm{J_{MP}} \times (28 - \mathrm{T})] \times \mathrm{V_{MP}} + [\triangle \mathrm{V_{MP}} \times (28 - \mathrm{T})] \tag{2.4}$$

The factor 28 is defined by the temperature reference used at the laboratory. Note that solar cells operating below 28 degrees celsius will generate more energy than the calculated on the table 2.2.

As the equation is a function of temperature, it is necessary to analyze the energy production changes with it. By calculating the results from 28°C to 75°C, which is the maximum operating temperature, for the three we obtain

Solar Cell	Lab. Cond	30°C	40°C	50°C	60°C	70°C
Spectrolab	41.586	41.3175	39.9819	38.6578	37.3450	36.0445
Azurspace	40.3119	40.0497	38.7453	37.4515	36.1680	34.8958
SolAero	39.760	39.5527	38.4921	37.4326	36.0445	35.317

Table 2.3: different solar cells as a function of temperature supposing $1cm^2$ solar cell. *All data on mW*.

As can be seen on the plot 2.6, Spectrolab cells are still giving the best values for electrical generation for the whole temperature range, while Azurspace is overcome by SolAero at high temperatures (more than $50°C$).

Knowing the distance from the sun the equilibrium temperature for different solar cells can be determined with accuracy by knowing their values of absorptivity (α) and emittance (ε) for the top and the bottom sides. Then, the equatuion of thermal balance is:

$$T^4_{\mathrm{MAX}} = \frac{J_{\mathrm{S}}\,\alpha_{\mathrm{t}}}{\sigma(\varepsilon_{\mathrm{b}} + \varepsilon_{\mathrm{t}})} \tag{2.5}$$

$$T^4_{\mathrm{MAX}} = \frac{J_{\mathrm{S}}\,\alpha_{\mathrm{t}} + q_{\mathrm{I}}\,\varepsilon_{\mathrm{b}}\,\sin^2(\rho) + J_{\mathrm{S}}\,a\,\alpha_{\mathrm{b}}\,K_{\mathrm{a}}\,sin^2(\rho) - \eta\,J_{\mathrm{S}}}{\sigma(\varepsilon_{\mathrm{b}} + \varepsilon_{\mathrm{t}})} \tag{2.6}$$

Where: J_{S} is the solar flux received at the orbit, α terms refers to the absorption of the material (sub t means at the top side and sub b means bottom side), β terms refers to the emittance (with the same meanings at the sub index), q_{I} is the energy balance expressed as: ($q_{\mathrm{i}} = q_{\mathrm{incident}} + q_{\mathrm{reflected}} + q_{\mathrm{transmitted}}$), a means the albedo, K_a is an empiric expression function of ρ ($0.664 + 0.521\rho + 0.203\rho^2$), η is the solar cell efficiency, σ is

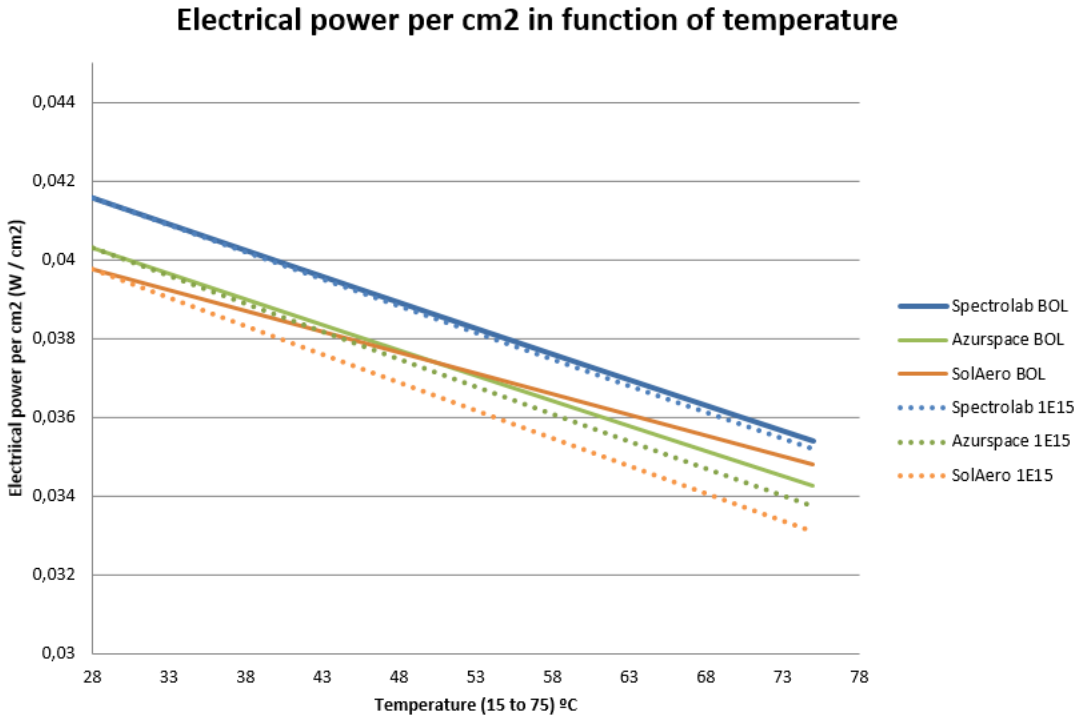

Figure 2.6: Generated power for different solar cells per unit area. Dashed lines represents the aggravation of the temperature degradation as a function of radiation of 1×10^{15} 1 MeV fluence.

the Stefan–Boltzmann constant ($5.67051 \times 10^{-8} W m^{-2} K^{-4}$), and finally ρ is the angle of incidence.

The equation (2.6) can be simplified by neglecting some terms. First of all the equilibrium temperature, by definition, implies a balance of energies $q_{\mathrm{i}} = 0$ deleting the whole second term. Moreover, the angle of view is $\sim 0^{\circ}$ and therefore $sin^2(\rho) \ll 1$. Third term of the equation involves the energy received from the Earth, understood as a black or grey body. It can be also neglected by arguing the large distance from the Earth to the solar sail, adding then just a relatively small energy radiated by the Earth. Moreover, on this term also appears the term $sin^2(\rho)$ which, again is ~ 0.

By applying all those simplifications to (2.6):

$$T_{\mathrm{MAX}} = \sqrt[4]{\frac{J_{\mathrm{S}}\,\alpha_{\mathrm{t}} - \eta\, J_{\mathrm{S}}}{\sigma \times (\varepsilon_{\mathrm{t}} + \varepsilon_{\mathrm{b}})}} \tag{2.7}$$

The last term includes all the energy transformed by the solar cell directly to electrical energy and hence, not directly into heat.

At this point, the only element needed to compute the equilibrium temperature for the solar cells are the values of absorptivity and emittance for the top and bottom sides. Typical values for GaAs solar cells are: $\alpha = 0.91$ and $\varepsilon = 0.85$. At the bottom side, the last layer of the solar sail, is chrome with ε = 0.1.

But the real front part of a solar cell is not the GaAs material but the coverglass that

protects the cells from the outer space radiation. Qioptiq is space approved designer and manufacturer of cover-glasses to protect the solar cells to the radiation, on the appendix D is shown the data-sheet for the determination of real absorption coefficients.

By adding a cover-glass to the solar cell the efficiency will be reduced due to the fact that the own cover-glass catch some of the photons radiated by the sun. To avoid this, a greater transmission of the cover glass is required around the wavelength of maximum emission on the solar spectrum. Visible radiation comes at wavelengths from 380 to $780nm$. By looking at data-sheet we can see that this maximum values of transmission at this wavelength values are for CMX AR (anti-reflectance) for $600-800nm$ with transmission value of 97.5%.

The relationship between transmittance and absorption is described by the *Beer-Lambert Law* as: $\tau = 10^{-\alpha}$. Then, if the trasmissivity is 97.5%, the absorptivity must be of 0.011. In consequence, the real optical proprieties for the GaAs behind the cover-glass can be approximated to:

$$\alpha_{total} = \alpha_{solar\,cell} - \alpha_{coverglass} = 0.91 - 0.011 = 0.899 \tag{2.8}$$

With all the emittance and absorptivity determined, the equilibrium temperature (2.7) for different solar cells is:

Manufacturer	Absorption	Emittance	Efficiency	Temperature
Spectrolab	0.899	ε_t=0.85 ; ε_b=0.1	30.7%	$76.55°C$
AzurSpace			30.0%	$77.58°C$
SolAero			29.5%	$78.31°C$

Table 2.4: Equilibrium temperature for different solar cells

For all solar cells equilibrium temperatures are higher than the maximum operative rage. There exist different ways to maintain the cells as cold as possible. A possible option could be to increase the emittance bottom area by adding temperature dissipators working as a radiators: by increasing the emittance area the equilibrium temperature will decrease by a factor: $1/\sqrt[4]{\triangle Area}$ (but affecting only on the bottom surface). For example, increasing the radiation area by 2 implies a reduction on Spectrolab cells temperature to:

$$T_{MAX} = \sqrt[4]{\frac{J_S\,\alpha_t - \eta\,J_S}{\sigma \times (\varepsilon_t + \mathbf{2} \times \varepsilon_b)}} = 69.91°C \tag{2.9}$$

As the dissipation only affects to the bottom area and, at the same time, this area offers a low emissivity, the heat dissipation is not that high. Also, the fact of adding a heat dissipator will increase the mass and complicate the deployment. Therefore, this option is discarded.

Other way to reduce the operating temperature consists on increasing the emissivity instead of the area. This can be made by painting the bottom surface of the solar sail related

to the solar cells. The fact of adding a paint coat does not affect drastically to the deployment nor the total mass of the solar sail. Therefore, this is the chosen way in order to reduce the solar cell equilibrium temperature.

The paint used must be space qualified, and the selected one is Inorganic white AZ-93. With thickness of 5 $\pm$ 1.5 mils (0.127 $\pm$ 0.038 mm) offers thermal emittance of 0.91 $\pm$ 0.02. Re-computing the data of the table 2.4 with the new ε_b = 0.91:

Manufacturer	Absorption	Emittance	Efficiency	Temperature
Spectrolab	0.899	ε_t=0.85 ; ε_b=0.91	30.7%	$26.59°C$
AzurSpace			30.0%	$27.47°C$
SolAero			29.5%	$28.10°C$

Table 2.5: Equilibrium temperature for different solar cells by painting the bottom surface with inorganic white AZ-93.

Now, particularizing for the equation (2.7) at those temperatures, the power generated at the beggining of life (BOL) remains as: (J_S for 1.01 AU from sun is: $1360.8W/m^s$).

- Spectrolab: $0.04159W/cm^2 \rightarrow$ 100.56% respect lab. conditions.
- Azurspace: $0.04031W/cm^2 \rightarrow$ 100.17% respect lab. conditions.
- SolAero: $0.03977W/cm^2 \rightarrow$ 99.98% respect lab. conditions.

Arriving to the conclusion that, referring to the behaviour of the solar cells with the temperature, Spectrolab offers lower operating temperature due to the fact of having better efficiency values and, respectively, better efficiency results at BOL than the Azurspace of SolAero ones.

The deterioration of the solar cells due to the high temperatures are aggravated as the time passes due to the ionizing radiation experimented under space environment. This deterioration is shown at the figure 2.6 as the dashed lines.

As can be seen on the plot and on the numbers, the effects on the temperature coefficients along time due to the environmental radiation only affects significantly (at those temperature ranges) to SolAero solar cells.

2.2.4.3. Radiation degradation losses

The main determining factor of the EOL efficiency of a solar cell is the radiation which it will absorb during the whole mission; this radiation is defined by the orbit.

As the goal of this project is to study the effect on the magnetotail produced by the solar pressure, there is no exact data with empirical values for the radiation on this zone. So, in this subsection we will study a first approximation of the radiation values by using the ESA's space environment information system called *Spenvis*.

For this, the first step is to determine the orbits characteristics on *Spacecraft trajectories*. There, 1 year total mission duration was selected.

Due to the fact that coplanar elliptical circular orbit with focus on L2 is not a typical orbit, *Spenvis* does not allow to directly study this orbit. That is why *near Earth interplanetary* with 1.01 UA distance from the sun ($1.51 * 10^{10} km$ which is approximately the distance of L2 to the sun) is selected.

The results for this data on *Spenvis* are:

Coverglass thickness (μm)	1 MeV total equivalent fluences
0	4.042 E+15
76.20	8.806 E+13
304.80	2.365 E+13
762.00	7.698 E+12
1000.00	**5.787 E+12**
1524.00	3.718 E+12

Table 2.6: 1 MeV equivalent electron fluencies per square meter.

For 1 year duration at 1.01 AU from the sun (L2) and with 0.1mm cover-glass thickness (thickness for Qioptiq cover-glasses), the 1 MeV equivalent electron fluence radiation absorbed by solar cell is 5.787 $\times 10^{12}$.

The data-sheets give the degradation of solar cells as a function of 1 MeV equivalent electron fluences as:

Fluence	3 E+13	1 E+14	2.5 E+14	5 E+14	1 E15	3 E15	1 E 16
Spectrolab	-	-	-	0.88	0.85	0.75	0.65
Azurspace	-	-	0.97	0.94	0.90	-	-
SolAero	0.96	0.95	-	0.91	0.89	0.86	0.82

Table 2.7: Datasheets data for solar cell degradations as a function of 1 MeV equivalent electron fluencies per square meter.

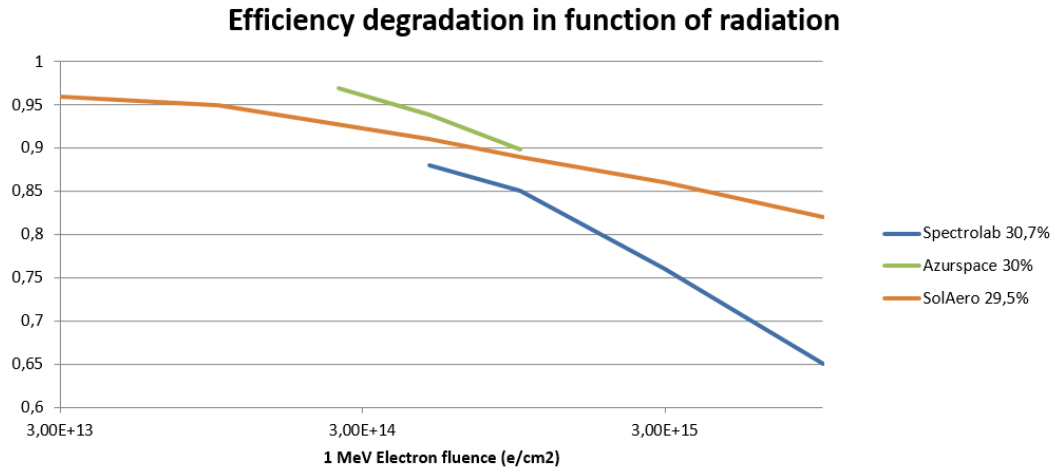

Figure 2.7: Datasheets data for solar cell degradation as a function of 1 MeV equivalent electron fluencies per square centimetre.

The empty fields on table and plot are due to the lack of information on data-sheets.

On this case, making a difference from the temperature losses, Azurspace presents better performance for low radiation levels, while SolAero presents more constant value of degradation along all fluences. Finally, Spectrolab offers the worst data by reducing the efficiency on a 45% when solar cell receives 1×10^{16} equivalent 1 MeV electron fluence.

As the range of study for the solar cells is focused on higher radiation values or long-term missions (from 3×10^{13} to 1×10^{16} e/cm^2). An approximation is needed to study the degradation at the lower radiation values ($5.787 \times 10^{13} e/cm^2$) found with Spenvis.

Supposing that the value of degradation at very low radiation is only the 1% can be added the point: 0.99 on 1×10^{8}, letting the plot as:

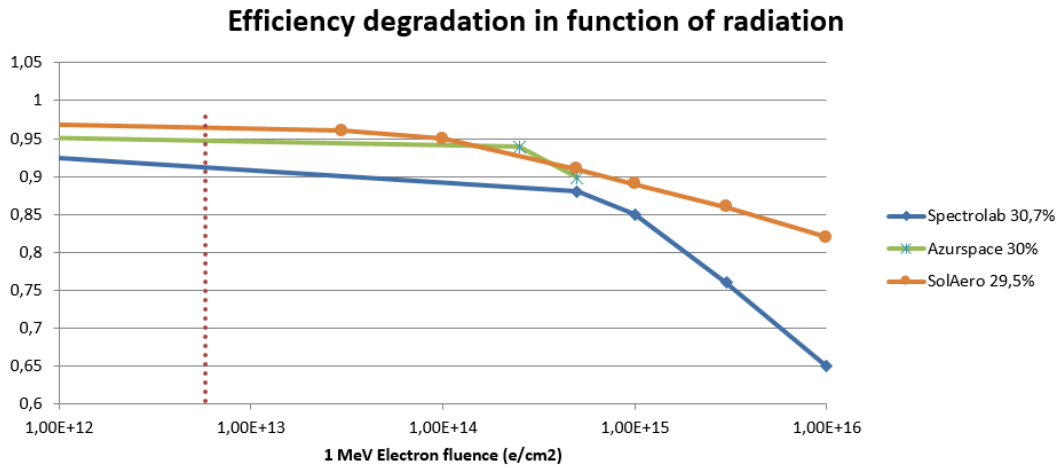

Figure 2.8: Approximation to low radiation Solar cell degradation.

With this data we can now interpolate for the radiation value for the different cells considered in this analysis:

- Spectrolab: 0.915%
- Azurspace: 0.970%
- SolAero: 0.945%

Concluding that Azurspace is the best option in radiation terms for the goals of the mission.

2.2.4.4. Angle of illumination losses

One of the more deteriorating factors on the efficiency of electric energy generation for solar cells is the angle of illumination (q). This angle is formed between the normal vector of the plane that conforms the solar cell and the direction of the solar radiation. Ideally, this angle forms near 0° by using a mechanical system to redirect the cells as a function of sun sensors readings.

On this project, the usage of this type of mechanizing is not viable due to the mass and structural limitations. Whence, the angle of illumination is the same as the solar sail inclination and, at the same time, this angle depends on the attitude determination and control sub-system. Whereby, the generation of the energy is function of the point on the orbit that the spacecraft is.

Typically, for small angles of illumination, the efficiency of the solar cells can be approximated as the cosine of this angle. But, for larger angles, where they start to appear reflectivity components, this expression gets far more complex. One of the empirical models express the variation of the reflectivity with the angle of illumination as:

$$r = -0.369\cos^3(q) + 0.637cos^2(q) + 0.750cos(q) - 0.015 \tag{2.10}$$

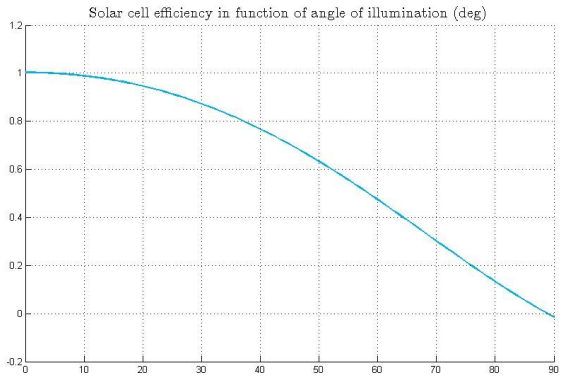

Figure 2.9: Graphical representation of the equation (2.10) on Matlab. Reflectivity factor vs angle of illumination for the first 90 degrees.

2.2.4.5. Eclipse losses

When some body (in this mission, the Earth or the Moon) stands between the spacecraft and the sun it is produced an eclipse. On this period of time, solar cells stop producing energy and the temperature decreases suddenly (on (2.7) the term J_S becomes 0).

The segments of the orbit where the eclipse occurs only depends on the geometry of the orbit and it can be calculated graphically. On this subsection it will be used *SolidEdge ST8 Academic Version* in order to graphically determine the eclipses on the orbit. The data taken for the draws are:

- Sun - Earth distance: 149.597.871 km
- Earth - L2 distance: 1.500.000 km
- Sun diameter ($\oslash_S$): 1.391.400 km
- Earth diameter ($\oslash_E$): 12.742 km
- Orbit diameter $\oslash_{L2}$): 300.000 km

During an eclipse period two types of shadows are generated: umbra, related to total eclipse, and penumbra, related to partial eclipse. The first one is that point or segment on the orbit where it is not possible to see any part of the sun. On the other side, penumbra occurs when it is not possible to see the totality of the sun and therefore, can not use the totality of his energy, but a portion of it is visible at the solar sail position.

Graphically, the umbra occurs when the projected shadow from the North Pole of the sun coincides with the north pole of the Earth and the south pole of the sun with the south pole of the Earth. On the other side, the penumbra occurs on the shadow cone generated by the opposite poles (See figure 2.10).

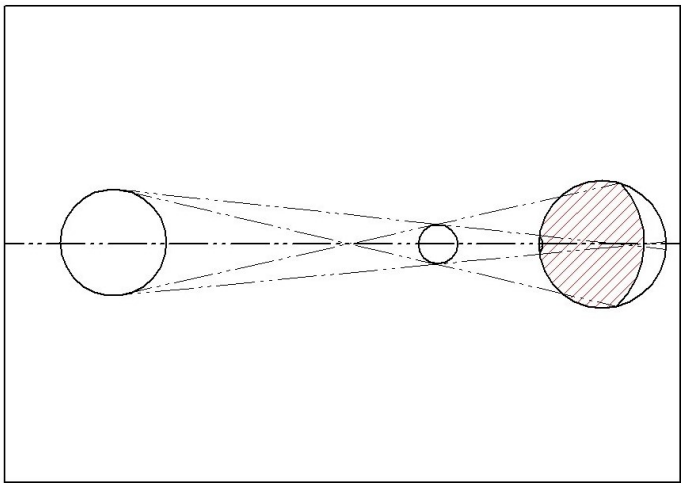

Figure 2.10: Eclipse example drawn on SolidEdge. Black inner zone represents total eclipse or umbra and outer red zone represents partial eclipse or penumbra.

Dimensionalizating for the mission data:

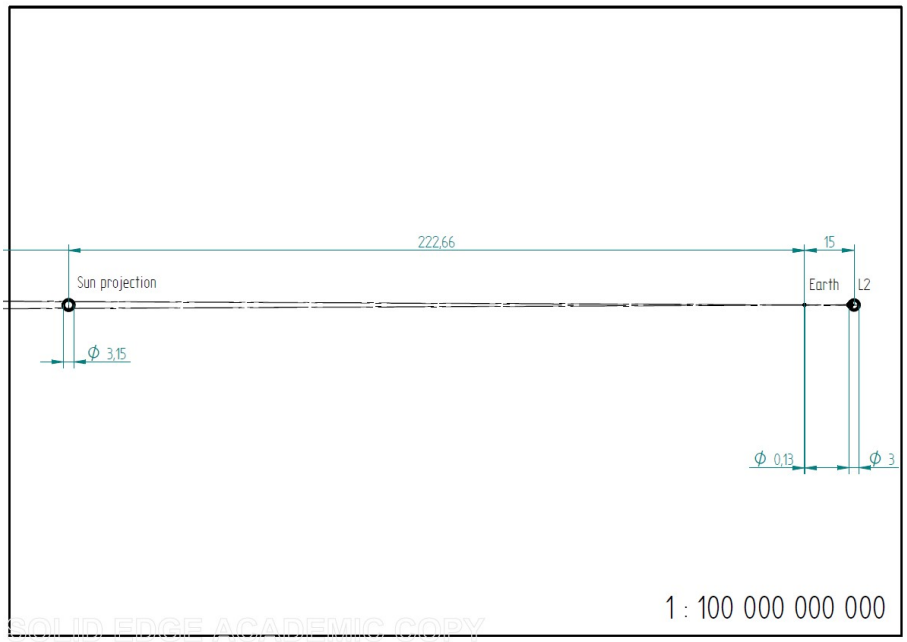

Figure 2.11: Graphical representation of the solar eclipse, at the left is the sun projection, followed by the Earth and finally the orbit over L2.

Notice that the sun is represented as a projection of it due to the impossibility of matching the horizontal scale to the radius on the Earth and its orbit.

By amplifying the previous figure on 40x factor to visualize better the effect of the eclipses on the orbit:

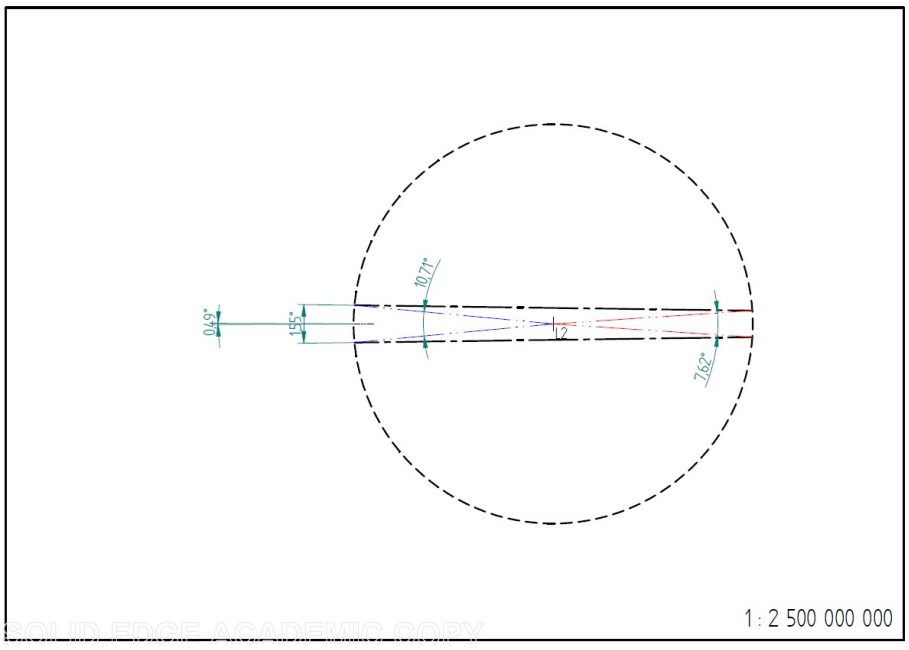

Figure 2.12: Graphical representation of the solar eclipse, amplifying the previous figure on factor 40 over orbit area.

With the angles obtained on the last figure can be determined the percentage of orbit that the spacecraft will be on partial or total eclipse by:

$$Total\,eclipse : 0.05^{\circ}(0.01\%) \tag{2.11}$$

$$Partial\,eclipse : (10.71^{\circ} + 7.62^{\circ}) - 0.05 = 18.28^{\circ}(5.078\%) \tag{2.12}$$

$$No\,eclipse : 360^{\circ} - (18.28^{\circ} + 0.05^{\circ}) = 341.67^{\circ}(94.908^{\circ}\%) \tag{2.13}$$

Whereby, suposing constant velocity for the whole orbit, the 94.908% of the time the solar cells are generating energy and the 5.078% generates a factor 0.5 (by average) at being on partial eclipse. The time on total eclipse is that small ($\gg 1\%$) that seems of small relevance.

$$94.908 + 0.5 * 5.078 = 0.97447\% \tag{2.14}$$

Then, the energy generation on a whole orbit is 0.97447 times the energy generated without eclipses.

2.2.4.6. Final dimensionalization

This subsection is a briefing on the previous subsections where we will be discuss the sizing on the solar cells needed to generate the required power at BOL and EOL.

As the first point, we consider the energy generated per surface area for the different solar cells at ideal conditions, which are:

- Spectrolab: $41.76 mW/cm^2$
- Azurspace: $39.34 mW/cm^2$
- SolAero: $38.92 mW/cm^2$

Then, by joining all the efficiency reductions discussed before, the generated power at EOL is:

	Temperature	Radiation	Illumination Angle	Eclipse	EOL
Spectrolab	1.0056	0.915	<0.8	0.975	$29.971 mW/cm^2$
AzurSpace	1.0017	0.970			$29.815 mW/cm^2$
SolAero	0.9998	0.945			$28.682 mW/cm^2$

Table 2.8: Final dimensionalization for different solar cells for 1 year at 1.1 AU from the sun.

Finally, by taking into account all the in-efficiency factors, Spectrolab offers better BOL and EOL energy production. The power that can provide the Spectrolab 30.7% solar cells at the EOL and by applying all the reductions discussed is:

$$29.971 \text{ mW/cm}^2 \times 1 \text{ hour} = 29.971 \text{ mWh / cm}^2$$

As will be detailed below, the consumption by the main bus without taking into account the communication sub-systems is 611.1 mWh. Then,

$$\frac{611.1\,mWh}{29.971\,mWh/cm^2} = 20.39\,cm^2$$

This means that it is needed at least 20.39 cm^2 to fed the main solar sail bus without taking into account the solar cell area needed to charge the battery which will be in charge of supplying energy to the burst based communications subsystem, as well as to the bus during the eclispe periods. As the smallest cell offered by Spectrolab is 27 cm^2 it is proposed to use as the main and only power source the Spectrolab 30.7%, 27 cm^2 solar cell (detailed the dimensions are given on *annex A*).

2.3. Energy storage

The maximum electrical consumption on the solar sail will vary from 240.5 mW and 1890.5 mW as a function of the communication subsystem status. Then, EPS must provide the energy needed for all no-communication subsystems leaving a margin in order to full charge the battery for the burst.

The solar sail will have two states of consumptions as a function of time. On one hand we have the fix consumptions related with the attitude and determination system, the payload and OBC which must be always turned on to ensure the correct behaviour of the spacecraft, note that, for having more conservative numbers, the computations above it will be taking into account a simultaneity factor of 1, that is, will be considered all the systems working at maximum capacity every time, except for RCDs which have 0.5 simultaneity factor because of there is no sense on active all of them at the same time. By the other hand we have the bursts on communication systems with a duty factor of 3.33% (2 minutes on for each hour) (see chapter 3).

Is the goal of the EPS to provide energy enough to cover the fix consumptions and divert part of the solar cell power to charge a battery that can provide the power needed on the burst.

On the following table 2.9 are shown all the consumptions for the solar sail.

2.3.1. Battery

One of the most difficults issues on the EPS design is the choice of a suitable battery, as due to the stringent mass restrictions it is needed an extremely light battery: ideally it should be less than 20 g. Most of the batteries used for conventional small satellites are still heavier than 100 grams, then making impossible to use a space qualified battery for the solar sail.

	Duty factor	Voltage (V)	Current(mA)	Power (mW)
Gyroscope (X, Y axis)	1	3.3	7.8	25.7
Gyroscope (Z axis)	1	3.3	6	19.8
Sun sensor	1	3.3	2	6.6
Accelerometer	1	3.3	0.002	0.007
Magnetometer	1	3.3	0.1	0.33
OBC	1	3.3	5.5	18.15
4x RCD	1	1	3 per cm^2	3 per cm^2
Communications	0.033	3.3	500	1 650

Table 2.9: Energy balance for all solar sail sub-systems.

It has also been studied the possibility of using a capacitor as a power storage device, but the option has been discarded by the impossibility to give energy for the two minutes burst whithin our mass restrictions. In this mission case, to fed the communication subsystems which have supply voltage of 3.3V at 500mA implies a capacitor size of:

$$\frac{0.5A \times 120s}{3.3V} > 18\, faraday$$

For example, a commercial 18 Farads capacitor (*CAP18* used to enhance low frequencies demand on audio systems) has a mass greater than 3 kg and a size of 28 x 20 x 8 cm.

Discarding space qualified batteries and capacitor as power storage system leaves only the option of using commercial batteries as our secondary (i.e., rechargeable) battery.

This option has been studied on previous missions. On December 2002 micro-satellite UNISAT-2 was launched by students of 'la Sapienza' (University of Roma) as scientific experiment by using commercial Li-ion battery as the main energy storage device for the whole satellite with two Ni-Cd battery packs as a backup.

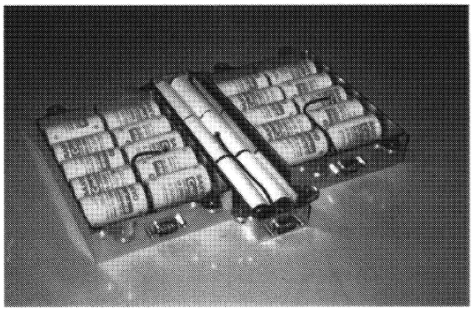

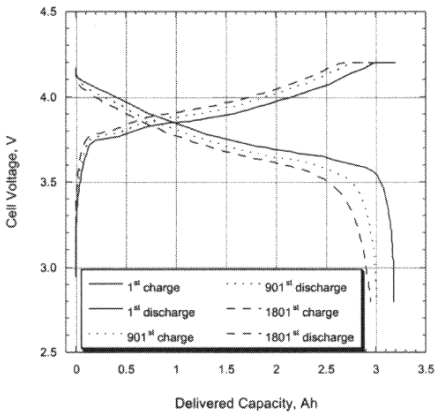

Figure 2.13: At the left, Battery configuration for the UNISAT-2 storage device, The Li-Ion (centre) and the two Ni-Cd (left and right) battery packs. At the right, the cell voltage vs delivered capacity as a function of the completed charge-discharge cycles.

At the right of the figure 2.13 are shown the charge / discharge curves for the 1^{st} to 1901^{st} cycles. As the differences between those curves is not much noticeable, they are supposed good enough to our case application at least for shallow depth-of-discharge (DoD) rates.

The selected batteries on UNISAT-2 were *SANYO*^{TM} *18650* from standard laptop computer. The specifications of this device are:

- Capacity: 3 500 mAh
- Nominal voltage: 3.6 - 3.7 V
- Charging voltage / current: 4.2 V / 1C
- Size: 65.3 mm (height) / 18.5 mm $\oslash$
- mass: 48 g

The cells selected on UNISAT-2 are still heavier than the ideal 20 grams battery for the solar sail. *SANYO*^{TM} *14500* is same family cells, this time smaller, with the following specifications:

- Capacity: 800 mAh
- Nominal voltage: 3.6 - 3.7 V
- Charging voltage / current: 4.2 V / 1C
- Discharging max. current: 1600 mA
- Size: 49.1 mm (height) / 13.85 mm $\oslash$
- mass: 20 g

By supposing the same, or similar behaviour on *SANYO*^{TM} *14500* as the *SANYO*^{TM} *18650* offered on UNISAT-2 (and still offering nowadays), *SANYO*^{TM} *14500* will be the selected battery.

2.3.1.1. Battery equilibrium temperature

The most limiting parameter on the battery performance is its operating temperature range. As the electronics are located at the sun facing side of the solar sail without any protective layer, the equilibrium temperature could reach high temperatures by reducing drastically the operative capacity and the life time.

For small spacecraft, from micro to femto satellites, most used mechanism in thermal control are passive elements in order to reduce as much as possible the electrical consumption. Also passive elements are light and easy to implement on most cases. One of the main passive thermal element are the reflectors or absorbers. There exist four types:

- Solar reflector ($\alpha/\varepsilon < 1$)
- Solar absorber ($\alpha/\varepsilon > 1$)

- Flat reflector ($\alpha/\varepsilon \sim 1$, with low α and ε)
- Flat absorber ($\alpha/\varepsilon \sim 1$, with high α and ε)

As the battery will be on the sun facing side the energy received from the sun will need to be reflected. Then, the element needed must have optical parameters fulfilling: $1 < \alpha/\varepsilon$. The selected material is aluminized Kapton.

Optical parameters for aluminized Kapton depends on the thickness used. The table below shows the absorbance and the emittance as a function of thickness.

Thickness	α	ε
0.08 mils	0.23	0.24
0.15 mils	0.25	0.34
0.25 mils	0.31	0.45
0.50 mils	0.34	0.55

Table 2.10: Absorbance α and emittance ε for aluminized Kapton as a function of thickness. Source: Appendix A: Surface Optical Property Data. Courtesy of NASA/GSFC.

By doing a first approximation to the equilibrium temperature of the battery, neglecting the conductive heat and supposing radiation as the only heat source, we can use the same equation used on solar cells for the computation of the temperature by neglecting the term related with the solar cell efficiency (2.7).

As the emittance for the top and bottom surface in this case is the same and assuming that the illuminated area is half of the total area, it is obtained the following equation:

$$T_{eq} = \sqrt[4]{\frac{J_S\,\alpha}{\sigma \times 2 \times \varepsilon}} \tag{2.15}$$

By computing the equilibrium temperature for the different optical proprieties associated with the different aluminized Kapton thicknesses it is obtained the following plot.

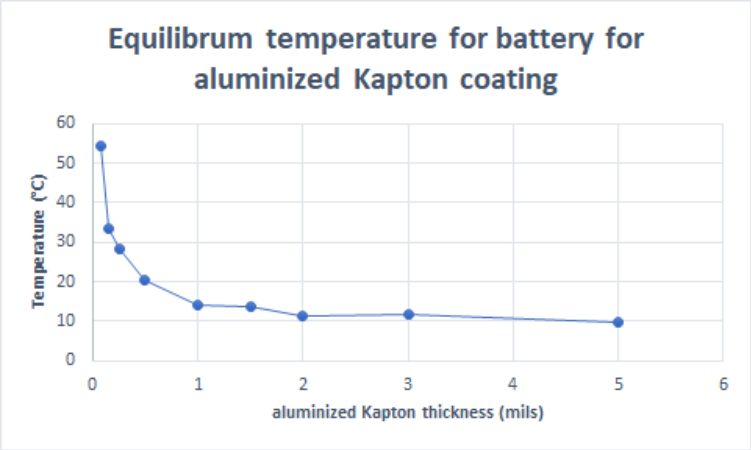

Figure 2.14: Equilibrium temperature of the battery as a function of the aluminized Kapton thickness.

On the left side of the plot it can be seen a huge difference on temperatures for the first 1 mils thickness. But it can also be seen that for 1 to 5 mils the temperature difference is drastically reduced.

On the next figure it will be shown the charge and discharge curves as a function of the operating temperatures for the selected battery *SANYO14500*.

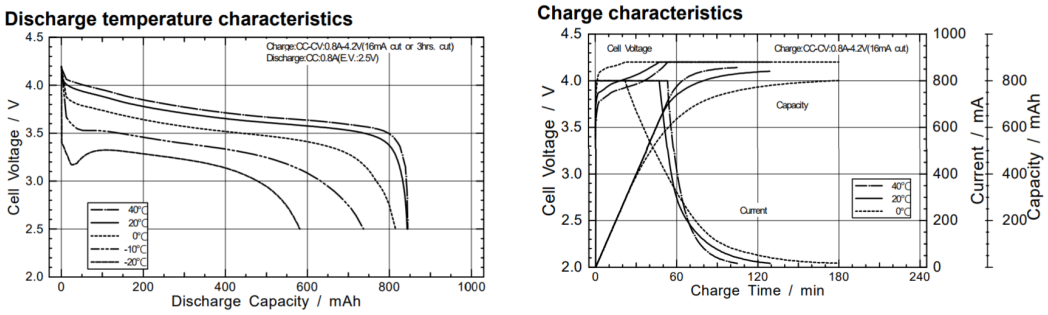

Figure 2.15: Charge (left) discharge (right) plots for *SANYO14500* as a function of the operating temperature

As we can see on the figure above, on the one hand, for high temperature ranges (about 40°C) the discharge on the cell is much shallower and efficient than for colder temperatures. But on the other hand, for the charging plot, the behaviour is the reverse, that is, the maximum efficiency in terms of time needed per charge is better for 0°C than for hotter one.

In conclusion, it can be said that the better operating temperature for the battery is at an intermediate point between the maximum and minimum operating temperature being about 20°C.

Now, by looking again at the figure (2.14), it can be determined that the needed thickness of aluminized Kapton to maintain the battery at approximately 20°C is 0.5 mils (0.0127 mm). The mass for this coating can be computed by knowing the density of the Kapton (1.42 g/cm^3) and the needed size of material. As the battery is a cylinder of heigh 49.1mm and 13.85 mm radius, the total surface of needed is: $2 \times \pi \times 49.1 \times 13.85 = 4\,273 mm^2 \rightarrow 54.26 mm^3$, letting the final mass of the coating to only 0.077 gr.

2.3.1.2. Discharge / Charge time analysis

The battery have the main function of being the unique power source during the communication bursts and eclipses. On the first case, the battery has to provide energy to the communication subsystem which operates at high current peaks 0.5 A in addition with the main load and the RCDs, making a total current consumption of 726.9mA (computed on Distribution section). Battery selected can provide maximum current of 1.6 A, so it will not be necessary to add any type of capacitors as burst support.

The electrical power in mWh consumed on the burst can be determined by knowing the duty cycle of 2 minutes over an hour as:

$$726.9 \text{ mA} \times 3.7 \text{ V} \times \frac{2}{60} = 89.7 \text{ mWh}$$

As the effective current used to charge the battery (computed also on distribution section) is 29.46 mA at charging nominal voltage of 4.2V, the time required to charge the battery after the communication burst is:

$$Charge\,time = \frac{89.7\,mWh}{4.2\,V \times 29.46\,mA} = 0.725\,h \sim 43.5\,minutes \tag{2.16}$$

The time needed to charge the battery after the 2 minutes burst is 43.5 minutes. As all the computations where made by supposing the worst case scenario (RCDs working at full capacity and power source at EOL) it is assumed than it is an acceptable value for charging time, thus validating the choice of the battery.

On the next figure are shown the battery fluctuations over the time.

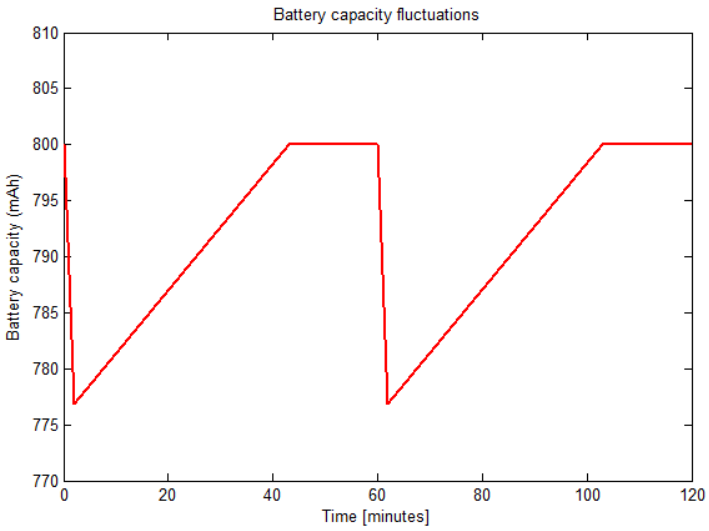

Figure 2.16: Battery capacity fluctuations over the time. Two cycles represented on the figure.

On the figure above it can be seen that the battery drain current rapidly at the burst by lowering the capacity from the maximum to 776.9 mAh in only two minutes. Then, by entering again on regular state (see Energy distribution subsection 2.4.1) the battery slowly recovers to 800 mAh after 43.5 minutes. Finally, the battery stops charging by opening the connection from solar cells and and remains at maximum capacity until the burst starts again repeating the cycle. Nevertheless, when fully charged, even active communication periods cause a shallow DoD, as will be discussed in the next section.

2.3.1.3. DoD

The capacity of the selected battery *SANYO*^{TM} *14500* is 800 mAh and the drained energy by the power subsystem is computed at the Burst state subsection (2.4.2) is 85.45 mWh, by working at 3.7 V that means 23.1 mAh. This means that the battery should never be under 775 mAh, fact that gives a very wide safety margin.

$$\text{DoD} = 100[\%] \times \frac{20.20\,mAh}{800\,mAh} = 2.887\%$$

2.4. Energy distribution

The energy distribution will behave in three different ways depending on the status of the transceiver (switch on or switch off) and the capacity of the battery at this moment.

Regular state will be when the transceiver is switched off and the battery needs current to charge. Periods when the battery is loaded but the burst has not yet started will be call standby states. Finally, when the transceiver switches on, it will be discussed as burst state. (see figure 2.16).

The states will be differentiated physically by three switches that would change their open or close state. the defined switches are shown on the whole bus at the end of this subsection (figure 2.4.3.).

- $S_1 \rightarrow$ Solar cell output
- $S_2 \rightarrow$ Battery input
- $S_3 \rightarrow$ Battery output

2.4.1. Regular state

Regular state is defined by:

- S_1 closed $\rightarrow$ Solar cell will provide energy to the main load.
- S_2 closed $\rightarrow$ Battery will use current from the bus to charge.
- S_3 open $\rightarrow$ Battery will not provide energy to the system.

The main load works at nominal 3.3 V, but the power source offers only 2.2 V at EOL. Then, it is necessary to add a boost voltage converter to feed the main load. Selected device is: *TPS 61200* low input voltage synchronous boost converter from *Texas Instruments*. This device provides a power supply solution by giving a continuous output fixed at 3.3V.

The boost converter *TPS 61200* will also be used as a first voltage booster stage to the charge of the battery. This fact will increase the charging time of the battery due to the device losses, but will ensure the correct behaviour and will avoid any type of peak current that could damage the battery.

The current that this device can supply is determined by the datasheet on figure 2.18. For 2.2 V voltage supply the maximum output current device admits is $\sim$800mA, when the input current is 429.6 mA. Thus, the current supplied by the solar cell is under the maximum admissible output current.

For perfect device the new current can be computed as:

$$V_{in} \times I_{\text{in}} = V_{out} \times I_{\text{out}} \rightarrow I_{\text{out}} = \frac{V_{\text{in}} \times I_{\text{in}}}{V_{\text{out}}} \tag{2.17}$$

$$I_{out} = \frac{2.194 \times 429.6}{3.3} = 285.62\,mA \tag{2.18}$$

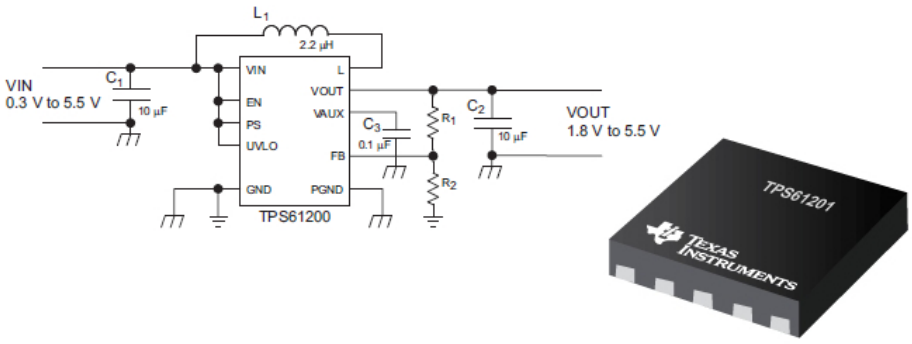

Figure 2.17: Electrical schematic and overview of *TPS 61200* low input voltage synchronous boost converter for *Texas Instruments.*

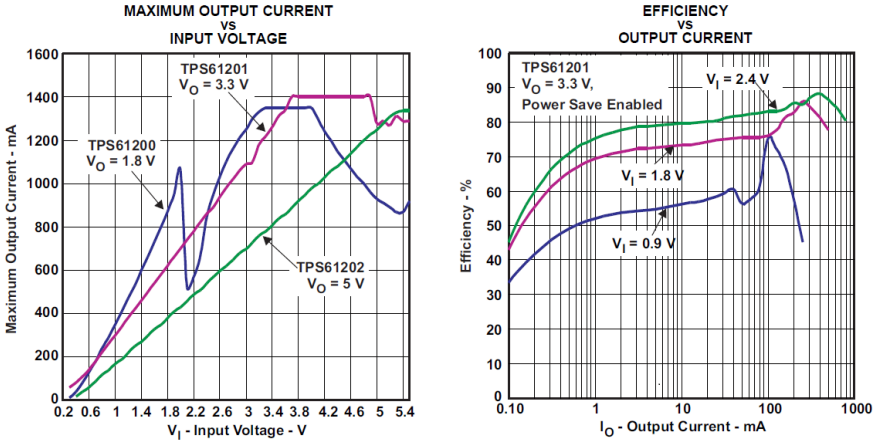

Figure 2.18: TPS61200 characteristics. At the left: maximum output current as a function of input voltage. At the right efficiency as a function of output current and input voltage.

But the device is not perfect, the efficiency is plotted again on figure 2.18 (right). By looking to the figure, for output current of 285.6 mA and input voltage of 2.2 V the efficiency can be approximated to 85%. This changes the equation (2.17) to:

$$I_{\text{out}} = \eta \frac{V_{\text{in}} \times I_{\text{in}}}{V_{\text{out}}} \rightarrow I_{\text{out}} = 0.85 \frac{2.194 \times 429.6}{3.3} = 242.78mA \tag{2.19}$$

This means that the available current for the main load is 242.78 mA. The main load includes: a 3-axis gyroscope, sun sensor, magnetometer, accelerometer and OBC. Total drained current for this devices is 21.4 mA. Therefore, it lefts 221.38 mA to the RCD and for charging the battery. By supposing a minimum deviation of 50 mA to charge the battery it lefts 171.38 mA to the RCD's.

As the RCD's from the attitude and determination systems only work at 1 V in series with two transistors of drop voltage 0.6V, it will be necessary again to convert the voltage. This time it will be easier as the voltage needs to decrease from 3.3V to 2.2V. For this,

TPS6222x from *Texas Instruments* is chosen. *TPS6222x* is a synchronous step-down converter with input voltage from 2.5V to 6V and configurable output from 1.2V to 2.3V. The maximum current output is 400 mA, so it can operate under our power requirements.

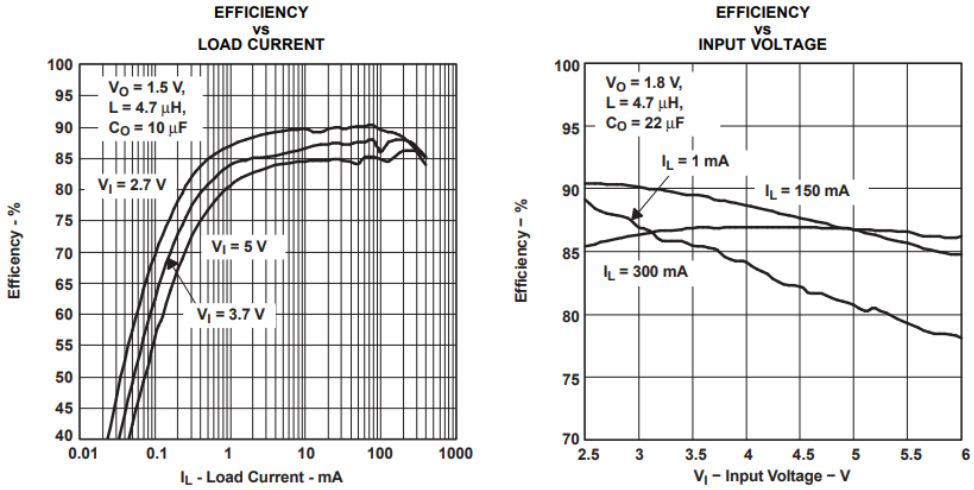

Figure 2.19: At the left, efficiency as a function of load current. At the right, efficiency as a function of input voltage.

On the figure 2.19 the efficiency of the regulator is shown as a function of load current and input voltage for voltage outputs of 1.5V and 1.8V. The datasheet does not offer the efficiency plot for 2.2V, but it will be approximated from those two shown. At the left plot (with output voltage of 1.5V), for V_I = 3.3V and I_L 171.38 mA the efficiency is between 85% and 90%, meanwhile on the right plot (with output voltage of 1.8V) the efficiency for the same values is also between 85% and 90%. Therefore, it is supposed that the efficiency for the 2.2 V will be in worst case 85%.

By applying the same equation as for *TPS61201* (2.19):

$$I_{out} = \eta \frac{V_{in} \times I_{in}}{V_{out}} \rightarrowtail I_{out} = 0.85 \frac{3.3 \times 171.38}{2.2} = 257.1mA \tag{2.20}$$

That means that the system is able to provide 257.1 mA to the RCD at constant 2.2V. By supposing a factor of simultaneity of 0.5 (just 2 out of 4 RCDs simultaneously working), the RCD maximum consumption (3 mW / cm^2) leads to a maximum RCD surface of:

$$\frac{257.1mA \times 1V}{0.5 \times 3mW/cm^2} = 171.38\,cm^2 \rightarrow 42.84\,cm^2 \text{ each one.}$$

The battery also needs a second stage booster as the charge nominal voltage is 4.2V, and a third one to reconverting the 3.7 V nominal voltage output to the 3.3 V to the main load and the communication sub-system.

Related with the voltage boost *RP601x*, a main load booster is selected: (*TPS61201*). This device is a buck-booster DC/DC converter which has an adjustable model where the output voltage could be from 2.75V to 4.2V feeded from 2.3V to 5.5V input.

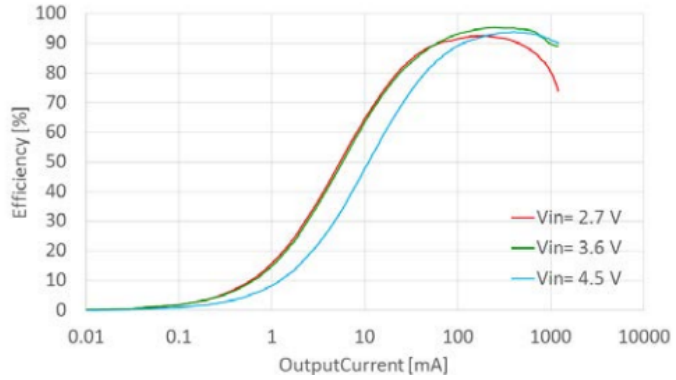

Figure 2.20: Efficiency as a function of output current for *RP601x* at different input voltage.

The efficiency for V_{in} = 3.3V and I_{out} = 50mA can be approximated well enough to 75%. Then, by applying the same equation as for *TPS61201* (2.19):

$$I_{\text{out}} = \eta \frac{V_{\text{in}} \times I_{\text{in}}}{V_{\text{out}}} \rightarrow I_{\text{out}} = 0.75 \frac{3.3 \times 50}{4.2} = 29.46mA \tag{2.21}$$

29.46 mA is the actual charging current provided to the battery at 4.2V.

2.4.2. Burst state

Burst state is defined as the opposite from regular state by:

- S_1 open $\rightarrow$ Solar cell will not provide energy to the main load.
- S_2 open $\rightarrow$ Battery will not use current from the bus to charge.
- S_3 closed $\rightarrow$ Battery will provide energy to the system.

The first step to provide energy to the whole bus is to adapt the 3.7 V nominal voltage to the 3.3 V at the main load. For this goal, the device selected is the step down 3.3 voltage regulator *Pololu S7V8F3*. The efficiency of the device as a function of output current and input voltage for 3.3 V output is defined on the following plot.

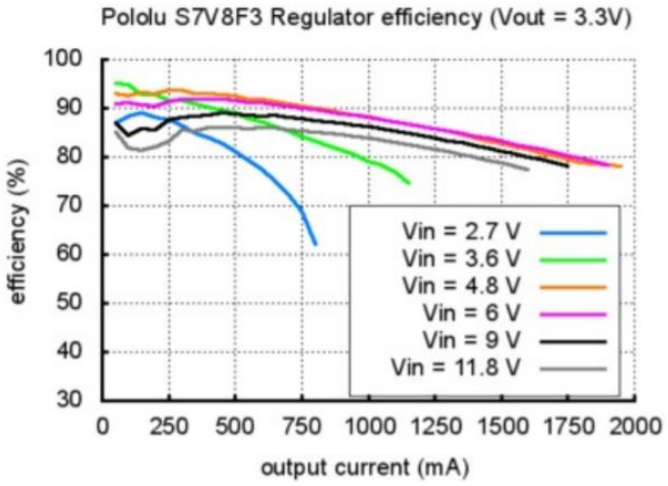

Figure 2.21: Efficiency as a function of output current (mA) of *RP601x* for different input voltages.

Drained current is 21.4 mA for main bus, 500 mA for the transceiver and 171.4 mA for the RCDs (before reconverted to operative 2.2 V), making a total of 692.8 mA, below of maximum limit. Then, by looking at the figure above, the efficiency of the device is 85%. Then, by applying the same equation than (2.21) but this time looking for the I_{in} and knowing I_{out}:

$$I_{in} = \frac{V_{\text{out}} \times I_{\text{out}}}{V_{\text{in}} \times \eta} \rightarrowtail I_{\text{in}} = \frac{3.3 \times 692.8}{3.7 \times 0.85} = 726.9mA \tag{2.22}$$

2.4.3. Standby state

Standby state is defined as the interval of time when the battery is fully charged and the system is waiting until the communication subsystem switches on:

- S_1 closed $\rightarrow$ Solar cell will provide energy to the main load.
- S_2 open $\rightarrow$ Battery will not use current from the bus to charge.
- S_3 open $\rightarrow$ Battery will not provide energy to the system.

This state basically ignores all the battery block and provides energy directly from the solar cell to the system. The viability of this state will not be demonstrated numerically as it is equivalent to the regular state but removing the current drained to charge the battery by leaving less restrictive situation.

By summarizing all those information into a block diagram scheme:

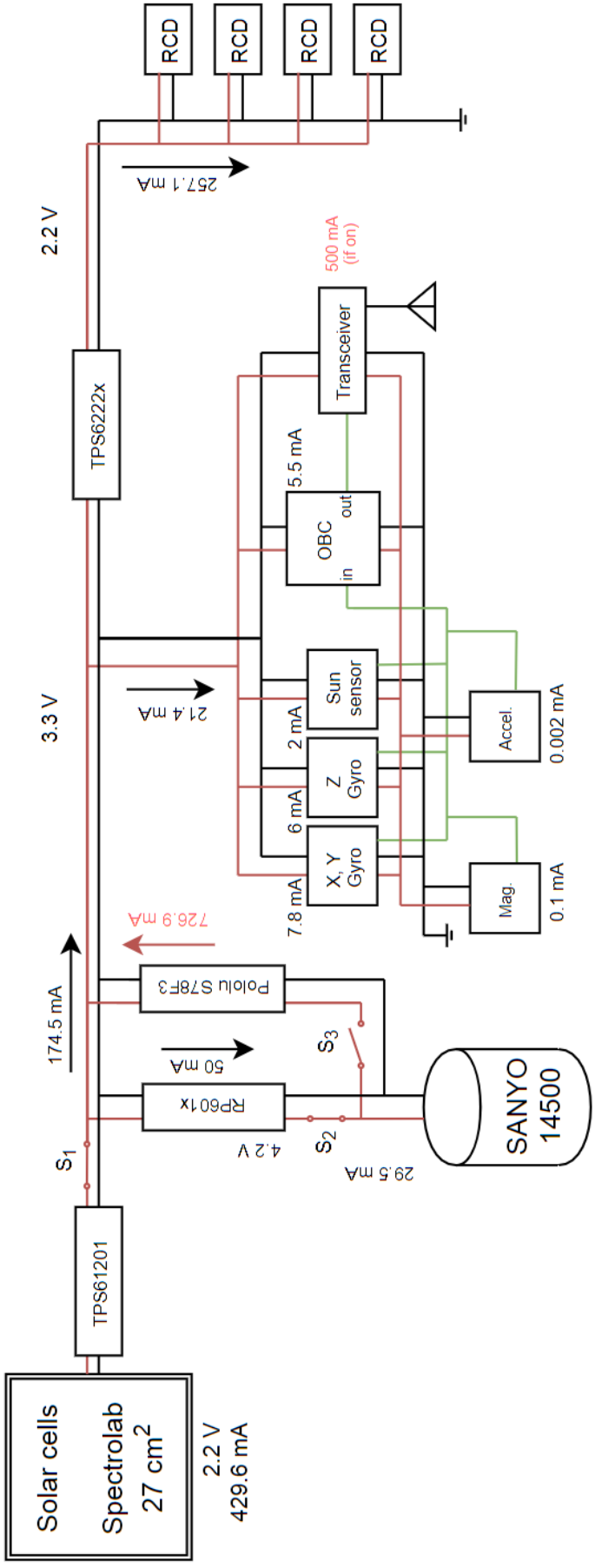

2.5. Electrical power subsystem conclusions

It has been shown that, with just a 27 cm^2 solar cell all the subsystems on-board the solar sail can be electrically fed, even at EOL, taking into account all the efficiency degradations by temperature, ionizing radiation, eclipse time and angle of illumination. Also, three switches have been implemented to protect and control the battery in addition of thermal coating to estabilize the temperature at ideal 20°.

The sizing and mass of all the elements used on EPS are listed below:

Device	**Size (mm)**			**mass (gr)**
Solar cell	69.1	3.97	0.23	2.268
TPS61201	3.15	3.15	0.80	0.028
RP601x	1.95	1.95	0.64	0.020
Polulu S78F3	17.78	12.7	2.54	5.67
LP3879	4.00	4.00	0.80	0.011
TPS6222x	3.05	3.05	1.1	0.006
SANYO 14500	49.1		13.85 ⊘	20
Battery coating				0.077
Total mass				**28.074**

Table 2.11: List of all the physical parameter of the elements conforming EPS.

CHAPTER 3. COMMUNICATION SUBSYSTEM

3.1. Introducction

A communications architecture is the arrangement, or configuration, of satellites and ground stations in a space system, and the network of communication links that transfers information between them. This chapter discusses this arrangement of links, their operation, and their effect on system design.

The solar sail communications is composed by a transceiver connected to a patch antenna which will relay all the data related with the position that the OBC computes, and the data gathered from the payload magnetometer (See chapter 1). The solar sail is unable to receive data from the exterior, that is why it must be fully autonomous.

There exist several requirements due to nature of the mission related with the electrical consumption and mainly with the mass. It is the goal of this chapter to determine this requirements in order to send all the needed data from the orbit to the ground station, and select the hardware which comply all (or the maximum number) of requirements.

3.2. Duty factor

Communication subsystem is the most power hungry system on the solar sail. As the power generation is limited by the small amount of solar cells (only $27cm^2$) which means a total production of 1276mW. This fact forces to use a burst communication system which is based on waiting until the battery gets fully charged and then establish communication for some minutes before battery runs out trying to minimize as much as possible the DoD (Depth of Discharge).

As has been seen in the previous chapter, by letting the battery charge for 45 minutes and sending all the required data in less than two minutes, the DoD is very shallow. Thus, the duty factor, assuming a communications link per hour, would be 2 minutes / 60 minutes = 0.0333.

3.3. Data rate

One of the main limiting factors on a satellite communication sub-system is the data rate. The amount of data that the system can carry decrease as the distance between the ground station and satellite grows. Then, it is necessary to determine the amount of scientific data that the solar sail generates and the data rate that it supposes (which will also depend on the duty factor).

As the mission goal is to determine the magnetic field in the magnetotial near the second Lagrangian point (L2), it will be needed at least to downlink the measurements from the magnetometer and the data related to the solar sail position and orientation. Those data depends on the data received by the attitude control and determination system which works with two gyroscopes (one for X and Y axis and other for Z), sun sensor and ac-

celerometer. With the data received for those sensors the OBS may be able to compute the position and orientation with enough accuracy.

Any point of the orbit can be determined by using spherical coordinate system (r, θ, φ), measured from the L2 position, where r is fixed to 1.5×10^5 km and φ to 0 degrees (circular orbit with no inclination) and θ will vary from 0 to 360 degrees. As the orbit will not describe a perfect circumference due to the possibility of several types of perturbations, a small quantity of bits will be reserved for the parameters r and φ. For both parameters will be supposed variation of ±10% which represents the ± 15000 km for range and ± 9 degrees for φ or orbit inclination.

To quantify the dynamic range it is necessary to determine the resolution wanted.

$$Dynamic\,range = \frac{Measurament\,range}{Resolution} \tag{3.1}$$

For 1000 meter resolution on three parameters can quantify the range as:

$$\theta = \frac{2\pi}{1000/1\,500\,000} = 9424 \leftrightarrow 14bits \tag{3.2}$$

$$\varphi = \frac{18\,\frac{\pi}{180}}{1000/1\,500\,000} = 471 \leftrightarrow 9bits \tag{3.3}$$

$$r = \frac{150\,000}{1000} = 150 \leftrightarrow 8bits \tag{3.4}$$

What means that are needed 14 bits + 9 bits + 8 bits (31 bits) to determine with resolution of 1000 meters for three axis the position of the solar sail on the space. As the magnetometer send the information on three axis it is important to know the orientation at the time of sampling. For this, as magnetometer is on the same plane as solar sail, we can send ADCS data associated with the orientation of the solar sail, the bits needed for these by 2 degrees resolution on each coordinate is:

$\ln_2$ (360/2) = 7.5 $\rightarrow$ 8 bits per axis.

Finally, 1 last bit is added to indicate if spacecraft is on eclipse period or not. For this, is needed to read the energy given by the solar cells, if this energy is below certain threshold means that spacecraft is on eclipse and this bit returns 1. In the opposite case, when the solar cells provides normal energy values, this bit becomes 0.

Summarizing all the data above and adding 16 bits for magnetometer, we got a total of 72 bits data information. To this bits it is needed to add the frame data, for serial communication it supposes 3 extra bit (start bit, parity bit and stop bit) for every 8 bit, or 1 byte data, following the next diagram:

Following a logical structure it will be split the data for every component in different bytes. For example, the data related with φ which got a dynamic range of 471 and needs 9 bits will be divided on two data bytes leaving blank (0) the remaining 7 bits. Then we got a final data rate of:

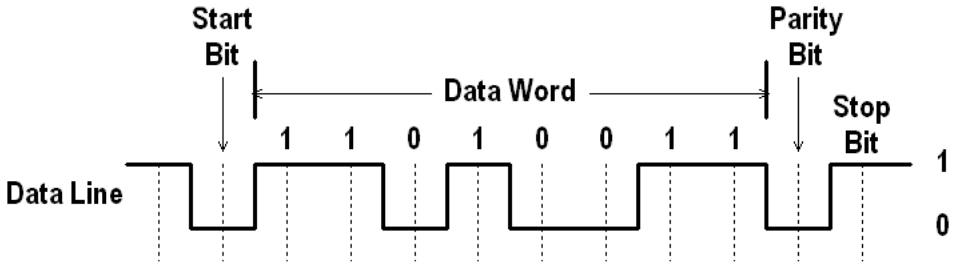

Figure 3.1: Serial communications bit stream diagram.

Parameter	Bits	Byte
θ	14	2
φ	9	2
Range	8	1
Pitch	8	1
Roll	8	1
Yaw	8	1
Eclipse	1	1
	Total	**9 Bytes**

Table 3.1: Necessary data rate for the determination of the position and the data related to the magnetic field

9 bytes imply 9 start, parity and end bits which adds up to a total of $9 * (8+3) =$ **99 bits**. Recording this data every second (1 Hz) for an hour implies a total of: $99\,bits * 1\,Hz * 3600\,seconds = 356\,400\,bits$. By introducing the duty factor we obtain a final data rate of:

$$\text{Data Rate} = \frac{356\,400\,bits}{120\,seconds} = 2\,970\,bits/s \rightarrow \sim \textbf{3 kbps}$$

Arrived at this point we can assume 3kbps as the minimum data rate needed by using simple serial communication but, serial communication has many inconveniences. For example, it does not have any type of address with what receiver antenna is unable to determine if the incoming message is from the solar sail transceiver or from another device.

Is for this reason that, following serial structure, AX.25 Amateur Packet Radio Link Layer Protocol was published by the American Radio Relay League (ARRL). On that document it is stablished the protocol used between two radios. This protocol is hugely used for amateur radio digital networks.

The fame structure for AX.25 protocol is:

Flag	Address	Control	Info	FCS	Flag
01111110	112/224 Bits	8/16 Bits	N*8 Bits	16 Bits	01111110

Figure 3.2: Frame construction for Information frame using AX.25 protocol.

Each field is made up of 8 bit (byte) as was considered before, but now the the start and end bits have been changed into two 8 bit *flags* delimiting the start and the end of the communication by using always the same combination ”01111110”, which are not allowed to occur anywhere else inside a complete frame.

On the Address field the source is identified, as is the destination of the message. And in the control field there is a check to see if the frame has been passed and control several attributes referring to OSI layers. The Frame-Check sequence (FCS) plays the role of the parity bit by ensuring that the message is not corrupted. This time, both the sender and the receiver calculate a 16 bit number that must coincide in order to give the message as good.

Finally, information field, in difference to the simple serial communication presented before, permits a total data capacity of 256 bytes (a total of 2048 bits), allowing to send much more information per frame.

By using AX25 protocol we can fill one frame each second by including on that frame all the information related with the magnetometer, position and date (summarizing 72 bits per second). This implies that we can compress the information for 28 seconds in only one frame ($28 * 72 = 2016$ bits < 2048 total available data capacity). Meaning that the whole hour information can be transmitted by using only 129 frames.

The new data rate remains as:

$$129 \text{ Frame} * (8 + 224 + 16 + 2048 + 16 + 8) = 297\,216 \text{ bits}$$
$$\text{Data Rate} = \frac{297\,216\,bits}{120\,seconds} = 2\,477\,bits/s \rightarrow \sim \textbf{2.4 kbps}$$

By using AX.25 protocol the communication system has been improved by adding more features on the message, by giving greater robustness, and by reducing the data rate almost a half.

3.4. Link equation

3.4.1. Friis equation theory

On a system there can only be a communication when the receiver antenna receives a signal strong enough from the transmitter antenna. The relation between the energy emitted and received is given by Friis equation:

$$P_{\mathrm{R}} = \frac{P_{\mathrm{T}}\, G_{\mathrm{T}}\, G_{\mathrm{R}}\, c^2}{(4\pi R f)^2} \tag{3.5}$$

Where, P_{R} is the received signal, P_{T} is the transmitted signal, G_{R} is the gain for the receiver antenna, G_{T} is the gain for the transmitter antenna, c is the speed of the light $(3 \times 10^8 m/s)$, R is the distance from both antennas and f is the operating frequency.

In order to decode the transmitted information the received power must be higher than a limit established as a function of antenna sensitivity, taking into account that the receiver antenna will receive information from other antennas operating at next frequencies (interferences) and some power due to the noise from different sources. To ensure that the

signal is good enough the energy-per-bit to noise density ratio (E_b/N_0) is introduced. Typically the minimum acceptable value for a good communication link is 5 dB, which implies that the received signal is at least 3.16 times greater than the noise.

Transmitter, as any other system, is not an ideal one. This is why line losses (L_l) are added to Friis equation. Apart from line losses, atmosphere gases attenuate the signal and reduce efficiency of communication link and need to be added to the link equation (L_a) (see figure 3.3). Finally, the operating temperature for the antenna changes the efficiency of it, so it is also added temperature losses (L_T).

By adding all this terms on Friis equation (3.5) and expressing the units on decibels:

$$\frac{E_b}{N_0} = P_T + L_l + G_T + L_S + L_a + G_R + 228.6 - 10\log(T_S) - 10\log(R)) \tag{3.6}$$

Where now, spreading losses and free space losses (L_S) are given by $(4\pi R)^{-2}$, or expressed in dB $10\log[(4\pi R)^{-2}]$.

3.4.2. Applying link equation

Before applying the link equation (3.6), we will briefly study the values for all the terms involved.

Energy per bit over noise (E_b/N_0) can be fixed, as it was said above, as 5 dB to assume a good communication link.

The gain for the receiver antenna, understanding it as the ground station, can be established by using the relationship between the effective diameter of the antenna with the gain:

$$G = \eta\frac{\pi^2 f^2 D^2}{c^2} \tag{3.7}$$

By supposing a parabolic antenna of 4 meters diameter with an efficiency of 0.70 working at a frequency of 2200 MHz, the gain of ground antenna is 43.76 dB.

We will assume that line losses are 3 dB, which is a generous margin as compared with reality. This assumption is due to the fact that line losses can not be determined on first approximation of spacecraft project because it depends of several factors, as the distribution or the wiring. 3 dB implies a factor 2 reduction and is supposed as worst case scenario.

On the other hand, spreading losses and free space losses (L_S) which only depends on the distance will vary from the $1\,350\,000$ km, giving -198.57 to $1\,650\,000$ km giving -200.31dB.

The atmospheric losses depend on the operating frequency. This is because at different frequencies electromagnetic waves can be absorbed or scattered by atmospheric components or weather phenomena. For example, rain droplet with a typical diameter of 2 millimetres interacts with electromagnetic waves of the same wavelength (see figure 3.3). Other aspect that affects the atmospheric losses is ground station's height and location.

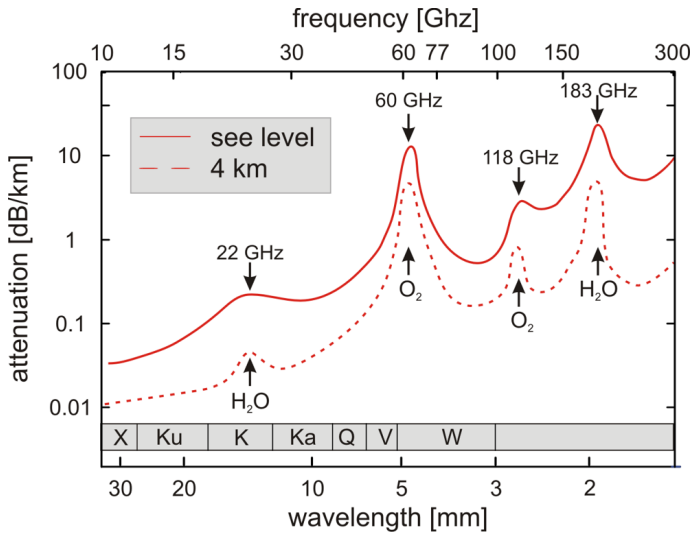

Figure 3.3: Atmospheric attenuation as a function of wavelength and ground station altitude.

For sea level ground station operating at 2.2 GHz, the signal attenuation due to atmospheric losses are $\ll 1$ and can be approximated to 0 dB.

For the term related with the operation temperature of the antenna, it will be assumed that the antenna temperature is the same as the solar sail structure calculated on the Thermal subsystem (299 K). Then, attenuation due to temperature is: -24.76 dB.

The last term, related with the data rate, was fixed to 2.4 kps on section 3.4.

All the data now is fixed except the terms related to the antenna on-board. The link equation (3.6) now can be resolved by keeping the G_{T} and P_{T} as unknown. The product of this two terms is known as the Effective Isotropic Radiated Power (EIRP).

$$EIRP = \frac{E_{\mathrm{b}}}{N_0} - L_{\mathrm{L}} - L_{\mathrm{S}} - L_{\mathrm{a}} - G_{\mathrm{R}} - 228.6 - 10\log T_{\mathrm{S}} - 10\log R \tag{3.8}$$

$$EIRP = 5 + 3 + 200.31 + 0 - 43.76 - 228.6 + 24.76 + 33.8 \tag{3.9}$$

$$EIRP = -5.49\,dB \tag{3.10}$$

Then, the required antenna needs at least an EIRP of -5.49 dB to establish communication on worst scenario case. (On previous calculations is selected the furthest point of the orbit at 1 650 000 km). This means that, for example, with radiated power of 100 mW (-10 dB) will be needed a gain of $G_{\mathrm{T}}[dB] = -5.49 + 10 = 4.51 dB$

3.5. Hardware selection

The goal of this section is to identify suitable hardware that meets the requirements above:

- EIRP $\geq$ -5.49 dB
- Data rate $\geq$ 2.4 kbps
- $E_b/N_0 \geq$ 5 dB
- Total mass $\leq$ 20 grams
- Electrical consumption (transmitter on) $\leq$ 2 W
- Preferred voltage supply at 3 - 5 V

The only hardware needed on the solar sail for the communication subsystem is the transmitter and the antenna. As the spacecraft must be able to carry on in orbit in an autonomous manner, it is not needed to have any type of receiver.

3.5.1. Transceiver

On the table above we show different manufacturers transceiver data:

Manufacturer	AMP	Syntronics	Endurosat
Name	FMT1 FSK	INST - 11b	S-band / UHF
Operating frec. (MHz)	433 - 2500	2200 - 2300	2400 - 2480
Max. bit rate	115 Mbps	500 kbps - 2Mbps	250 kbps - 2 Mbps
Current	190 mA	500 mA	1.35 A
Voltage	9 - 16 V_{DC}	3.3 V_{DC}	4.75 - 5.25 V_{DC}
Input power	4.77 dBW (3 W)	2.17 dBW (1.65 W)	8.29 dB (6.75 W)
Output power	+24dBm (250 mW)	+25.2dBm (330 mW)	+33dBm (2 W)
mass (gr)	34	2	114
Size (mm)	31.75 x 63.5 x 9.53	20mm diameter	90.2 x 95.9 x 25.2

Table 3.2: S-band low-power transceiver list.

The very large amount of S-band transceivers have typically a mass over 100 g, as the Endurosat shown on the table. The only transceiver that comply with the mass requirement is INST - 11b from Syntronics. In addition, comparing this with FMT1 FSK from Advanced Microwave Product (AMP) we can see that the one provided by Syntronics gives much better performance, with a 20% efficiency compared with the 6.33% from FMT1 FSK. Also, Syntronics offers a perfect matching voltage in order to simplify the power distribution inasmuch as all the other sensors and components have a similar voltage supply. Therefore, INST-11b will be used as transceiver for the communication subsystem.

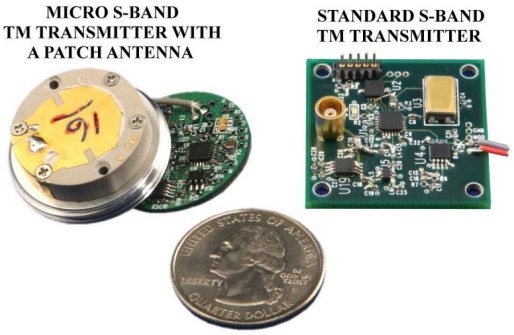

Figure 3.4: Low-power ultra low mass S-band transmitter INST-11b with a patch antenna (at the right).

The selected transmitter has an output power (P_{T}) of +25.2dBm = -4.81 dBW (330 mW). Taking into account that EIRP must be grater than -6.78 dB as is specified on the requirements at the start of this sections the antenna gain must have at least:

$$\text{-5.49 dB + 4.81} \sim \text{-0.68 dB}$$

3.5.2. Antenna

Microstrip or patch antennas are becoming increasingly useful because of their simplicity in terms of manufacturing and implementation. These low cost antennas do not provide the better gain performances, but gives approximately an omnidirectional radiation pattern. This type of antenna match perfectly with the behaviour of the solar sail which will be rotating as the attitude determination and control subsystem dictates and will by unable to focus a narrow communications beam.

Currently there exist low-powered antennas, but all of them with high mass. Due the non-existence of S-Band ultra-low mass patch antennas leads us to the conclusion that the only viable way of comply with all the requirements is by making it custom build. For this, a theoretical study will be carried out first and then a simulation by using software *ANSYS HFSS* to test the theoretical results and have an approximation for the antenna gains.

Microstrip antennas are made by three elements, the electromagnetic wave radiative element at the top (patch), a ground plate at the bottom and between those two plates a dielectric substrate. Dielectric substrate have typical width measures of $0.003 \geq \lambda_o \geq 0.05$ where λo is the wavelength for the resonating frequency of the own antenna. It is to say, for 2.2 GHz operating frequency (λ_o = 0.13636 m) the selected width can typically vary from 0.40908mm to 6.818mm. The selected width for the dielectric substrate will be fixed at 1.6mm, staying beyond the two limits.

There are numerous substrates used on the design and manufacturing of micro-strip antennas, typically those substrates haves a dielectric constant of: $2.2 \geq \varepsilon_r \geq 12$. Lower dielectric constant values implies larger antennas but also implies an improvement on the efficiency. It is because of this that there not exist a better substrate for every antenna. The selected substrate on this antenna will be one of the most popular inside design of patch antennas: Epoxy FR4 with relative permittivity of 4.4.

By fixing the width and the relative permittivity (or dielectric constant) of the substrate, the only variable is the radius of the patch. There exist a relation between all those parameters given by *Constantine A. Balanis* at "*Antenna Theory*" on *1982*.

$$a = \frac{F}{\left(1 + \frac{2h}{\pi \varepsilon_r F}\{\ln(\frac{\pi F}{2h}) + 1.7726\}\right)^2} \tag{3.11}$$

Where,

$$F = \frac{8.791 \times 10^9}{f_r \sqrt{\varepsilon_r}} \tag{3.12}$$

By considering the fringing effect. (Understanding fringing effect as the bulging of the electromagnetic flux lines due to the separation between two electrical plates, in this case ground and patch. This effect occurs often on capacitors). Can find the effective radius of the patch as:

$$a_e = a\left(1 + \frac{2h}{\pi \varepsilon_r a}\{\ln(\frac{\pi a}{2h}) + 1.7726\}\right)^2 \tag{3.13}$$

By applying all these equations to the data we obtain F and a.

First, for (3.12):

$$F = \frac{8.791 \times 10^9}{2.2 \times 10^9 \sqrt{4.4}} = 1.9049749 \tag{3.14}$$

Then, for (3.11) and (3.13):

$$a = \frac{1.9049749}{\left(1 + \frac{2\times 0.16}{\pi \times 4.4 \times 1.9049749}\{\ln(\frac{\pi \times 1.9049749}{2\times 0.16}) + 1.7726\}\right)^{1/2}} = 1.8528cm \tag{3.15}$$

$$a_e = 1.89\left(1 + \frac{2 \times 0.16}{\pi \times 4.4 \times 1.89}\{\ln\left(\frac{\pi \times 1.89}{2 \times 0.16}\right) + 1.7726\}\right)^2 = 1.906cm \tag{3.16}$$

At this point all the patch antenna data are determined as:

With all these data it is possible to simulate the performance for the patch antenna by using *ANSYS HFSS*.

Width	ε_r	Frequency	Radius	Effective Radius
1.6mm	4.4	2.2 GHz	18.528 cm	19.06 cm

The antenna will be fed with a coaxial SMA connector (to match with the selected transceiver). This connector will be placed slightly to the side of the patch, where the transceiver is located in order to reduce the wiring mass. Also, the substrate will be disk-shaped (again as the transceiver). For coaxial SMA connector will be used the material *pec (perfect electric conductor)*.

Out of theoretical computations, by try and error probes on *HFSS* simulator, it has been seen that the size of the substrate implies changes on the gain and in the radiation pattern. By increasing the substrate size (by keeping the heigh constant), the gain increases significantly but also the directivity. High directivity is a problem at the time on communications do the lack of antenna orientation system, then, the size must be small enough by ensuring the gain is high enough for satisfy the EIRP requirements fixed at the beginning of this section.

The radius of the substrate has been fixed, by trial and error iterations, to 22 mm matching, at the same time, with the size of the transceiver (20mm radius).

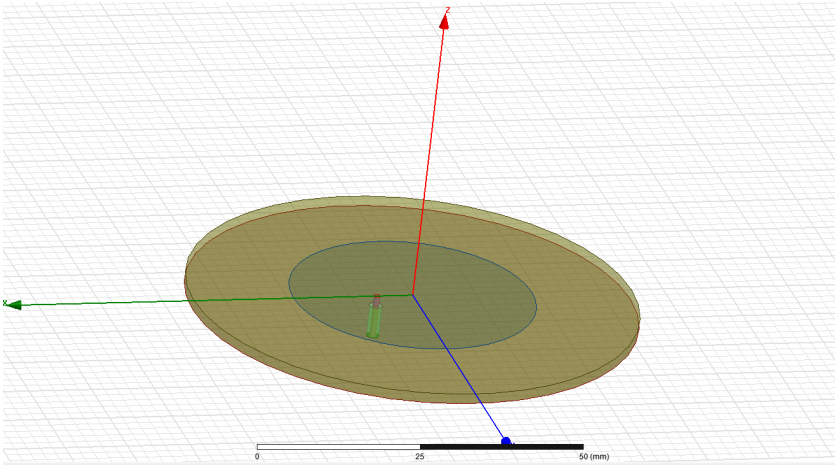

Figure 3.5: Circular patch antenna overview designed on HFSS Software.

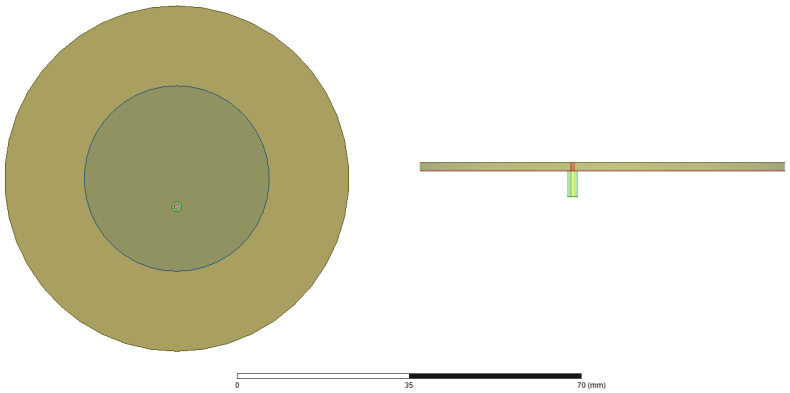

Figure 3.6: Top and lateral view.

All the elements are showed on the list above by showing the draw colours.

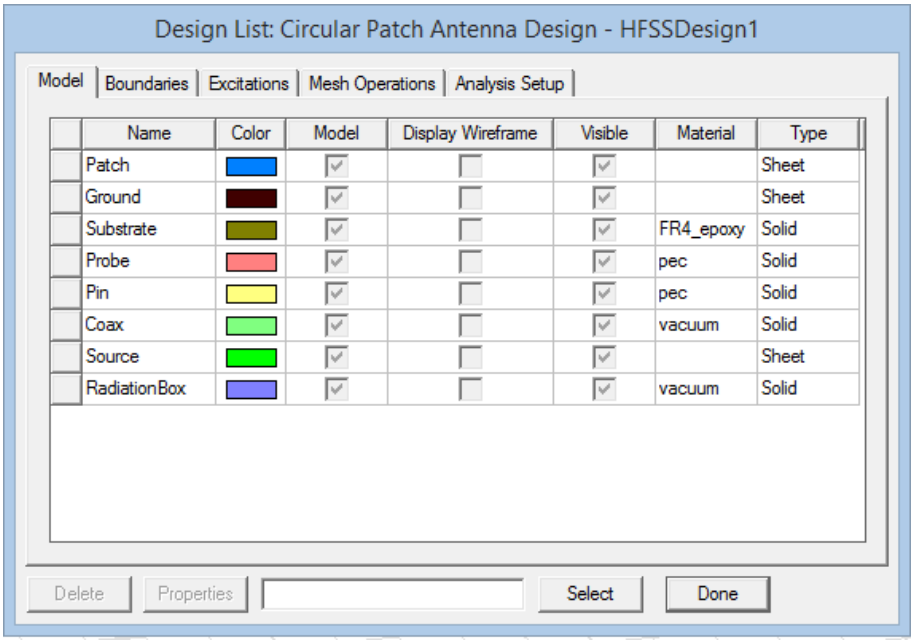

Figure 3.7: List of the elements conforming the circular patch antenna.

Patch, ground and substrate conforms the antenna itself. Probe, pin, Coax and Source make reference to the SMA connector and radiation box is hidden because of do not provide any design information.

By compiling and analysing the results from 1.5 GHz to 3.5GHz within 200 intervals

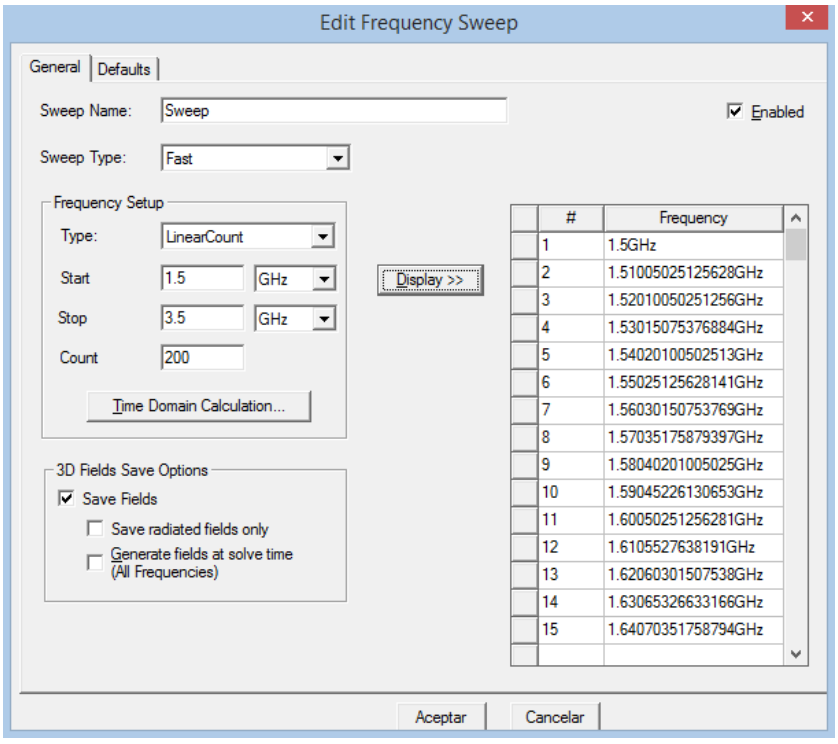

Figure 3.8: List of the elements conforming the circular patch antenna.

Results show that, effectively, the operation frequency is near 2.2GHz (exactly 2.18GHz).

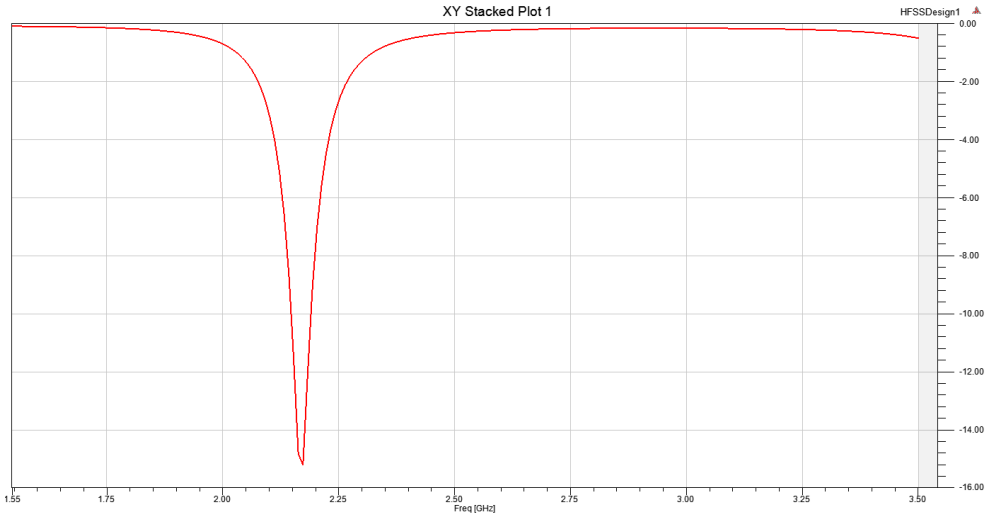

Figure 3.9: Resonating frequency for circular patch antenna.

With a gain radiation 3D plot pattern of:

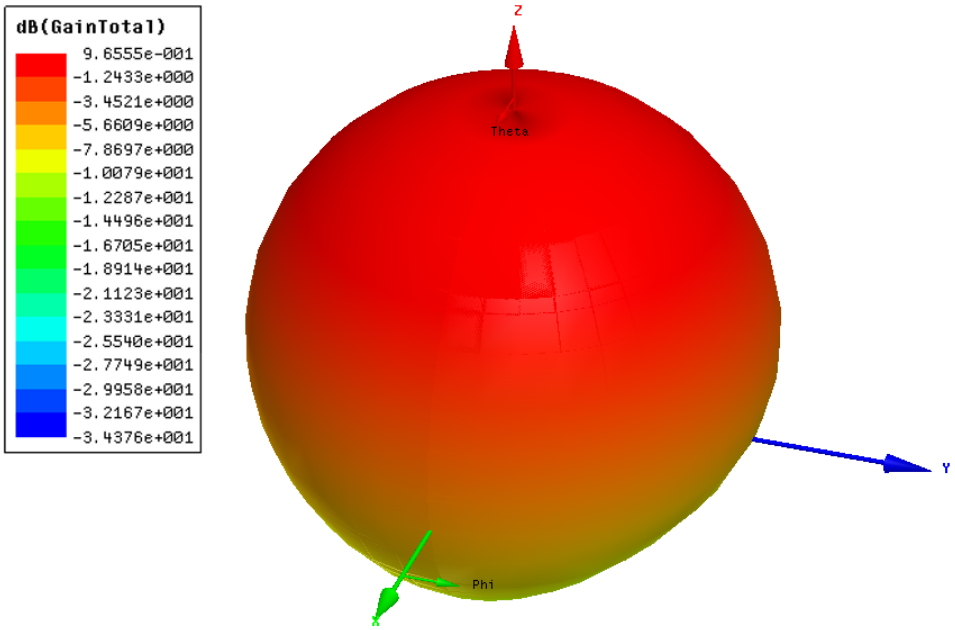

Figure 3.10: Gain radiation pattern 3D plot (in dB) top view.

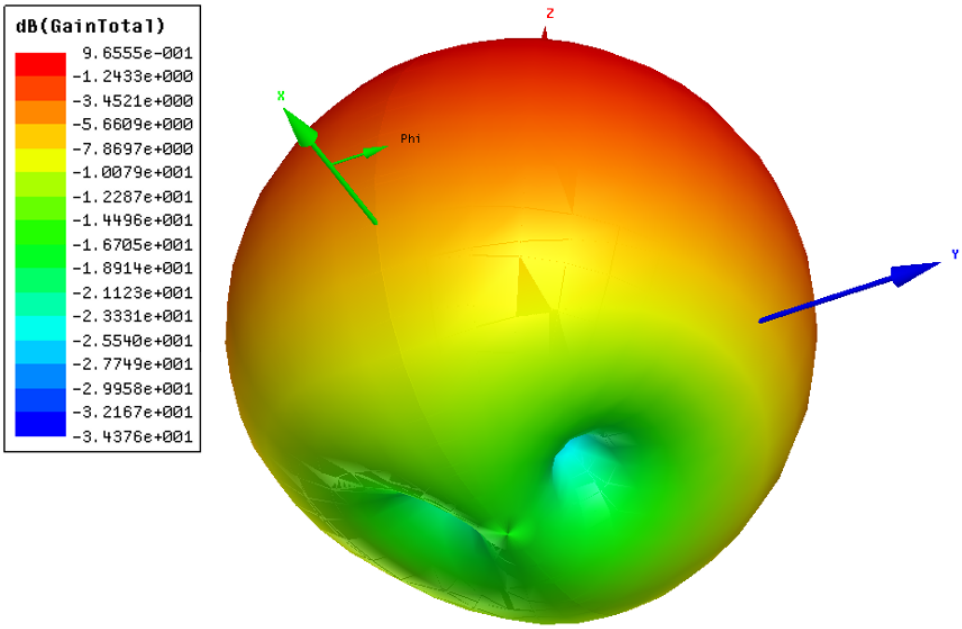

Figure 3.11: Gain radiation pattern 3D plot (in dB) bottom view.

With gain on cross section for angles phi and theta:

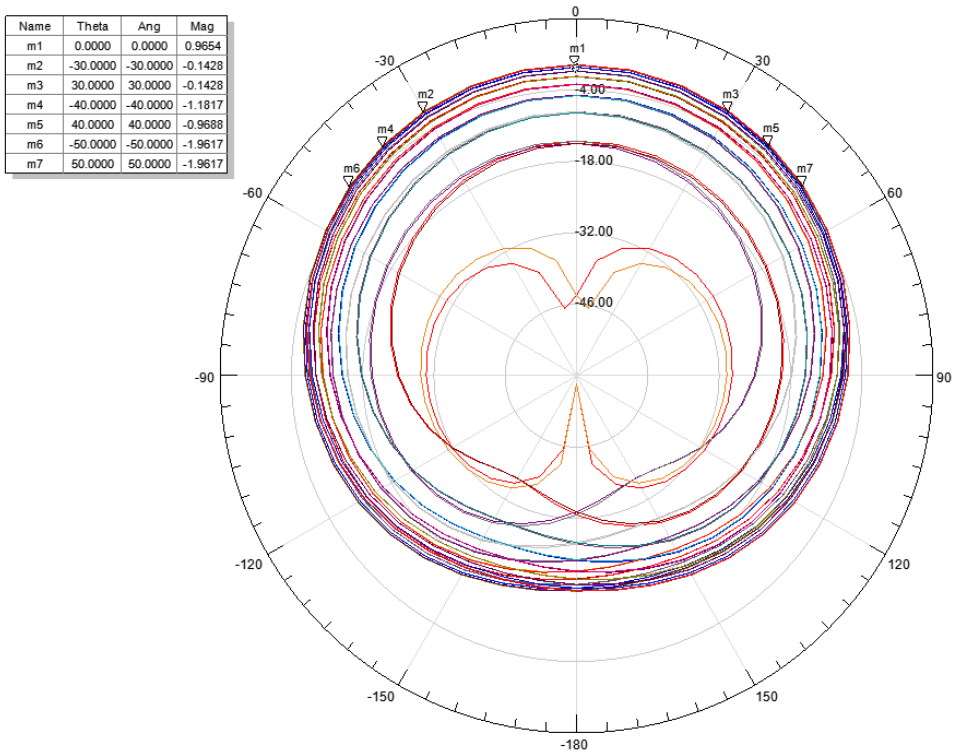

Figure 3.12: Gain (in dB) cross section for phi angles.

Recalling that the required gain must be greater than -0.68 dB, we can see at the figure above that this condition is fulfilled for angles smaller than $\sim$35 degrees.

At the maximum point of the antenna lobe, the gain is 0.97 dB. For the 25.2 dBm output power, the maximum EIRP of the system is:

$$\text{EIRP} = -4.81 + 0.97 = -3.84 \text{ dB}$$

By re-computing the link equation (3.6) it is obtained that actual signal to noise ratio is:

$$EIRP = -3.84 - 3 - 200.31 - 0 + 43.76 + 228.6 - 24.76 - 33.8 \tag{3.17}$$

$$EIRP = 6.65 > 5\,dB \tag{3.18}$$

The weight of the antenna can by easily determined by calculating the total amount of substrate volume as: $\pi \times a_e^2 \times h = \pi \times 1.906^2 \times 0.16 = 1.826 cm^2$ and pondering for the the density of the FR4 substrate is 1.9 gr/cm^2. This means that the antenna mass is 3.5 grams, by adding 5 gram for the coaxial connectors and wiring sums a total of 8.5 gram.

3.6. Communication sub-system conclusions

	Requirements	Actual data	Accomplish?
EIRP	$\geq$ -5.49 dB	-3.84	✓
Data rate	$\geq$ 2.4 kpbs	2.4 kbps	✓
E_b/No	$\geq$ 5 dB	6.65	✓
Total mass	$\geq$ 20 gr	8.5 gr	✓
Electrical max consumption	$\geq$ 2 W	1.65 W	✓
Voltage supply	*pref.* 3 to 5 V	3.3 V	✓

The table above shows the results for the communication subsystem design, which satisfies all the requirements and improves specially on the system mass. This fact would allow an improvement of the antenna performance by improving the data rate or the required power consumption on future project works.

CHAPTER 4. ON-BOARD COMPUTER

4.1. Hardware

The selected On Board Computer (OBC) for the solar sail is the microcontroller *ATmega328*. Microcontrollers are commonly used on CubeSats due to the low mass, power consumption, and price.

The main specifications for *ATmega328* are shown on the table below:

ATmega 328 specifications

Flash programmable memory	32 kBytes
EEPROM	1 KBytes
SRAM	2 KBytes
Speed grade$_{@\ 3.3V}$	10 MHz

ATmega328 has three types of memories associated for difference usages: Flash programmable memory, EEPROM and SRAM. As it is seen on the table above the largest memory is Flash programmable, this part is where the program is updated and stored, and hence it is no-volatile: the stored program will not disappear even if the power for the OBC were switched off. SRAM (Static Random Access Memory) is the second largest memory, and is the responsible for creating and manipulating the variables. Differently of flash memory, it is volatile memory, and then all the variables stored on SRAM will be deleted if the OBC switches off. Finally, EEPROM is the portion of memory destination to the long term storage software and variables. EEPROM, as flash memory, is not volatile.

It is required store all the data related with the position, time and magnetic field on the flash. On chapter 2 this data was quantified as 72 bits per second during one hour. This gives a total amount of 297 216 bits or 37.15 Kbytes. As the flash memory for the OBC is quite small (only 32 Kbytes, without counting code storage) external memory must be added to store all the data before the communication burst.

Selected device is *AT25DF512C* manufactured by *Adesto technologies*, it is a 64 Kbytes Flash memory is a serial interface Flash memory device designed for use in a wide variety of high-volume consumer based applications. It is compatible with SPI communication protocols and it requires a voltage supply between 1.65 and 3.6 V so it can be connected with the general bus as same as OBC.

By adding this external Flash memory the total amount of storage data increases to 64 Kbytes of non-volatile information, enough memory for storing all the data gathered by the experiment without need any type of data compression mechanism.

4.2. Communication protocols

OBC will be connected to a set of devices as inputs, which use different communication protocols and, therefore, the physical architecture must be adequate for each protocol. In addition, sun sensor gives analogic outputs, so and ADC converter will be needed.

All the discussion about the protocols and the data processing will be shown below.

Device	Protocol
X, Y Gyro Z Gyro	SPI
Accelerometer Magnetometer	I^2C
Sun sensor	Analogical

Table 4.1: Communication protocol for all Solar Sail input devices.

When input data is received, the OBC must process it and sent the relevant information to the output devices: RCDs and transceiver.

4.2.1. SPI

SPI (Serial Peripheral Interface) is often used as the synchronous communication protocol. It is based on the full duplex communication between master and one or more slaves.

SPI uses four signal lines:

- **SCLK** (Clock Signal): signal sent by the master to all the slaves. All SPI signals are synchronous to this clock signal.
- **MOSI** (Master Output Slave Input): Data line from the master to the slaves.
- **MISO** (Master Input Slave Output): Data line from the slaves to the master.
- **SS** (Selected Signal): Line to select the slaves that masters communicates with.

To stablish a communication master-slave, the SPI master selects the slave wanted to get the information from by pulling the $\bar{SS}$ signal corresponding to the slave low. Once the wanted slave is selected by the master, both activate and use the same clock signal (SCLK) synchronously, and generate information in full-duplex mode by using double physical channel (MOSI) for sending data from master to slave and (MISO) to send data from slave to master. (see figure)

4.2.2. I^2C

I^2C (Inter-Integrated Circuit), is also frequently used as a communication protocol based on multi-master, multi-slave architecture. I^2C consist on two signals: Serial Data (SDA) and the clock signal (SCL). Unlike SPI protocol, it does not exist any type of slave selection, but all slaves and masters are listening and writing at the same time. To make this possible, a few control bits must be added to identify the direction and the acknowledgement of the signal. This protocol, unlike SPI, have fixed maximum velocities to: 100 kb/s, 400kb/s, 3.4 Mb/s and, depending on the devices, 10 kb/s and 1 Mb/s.

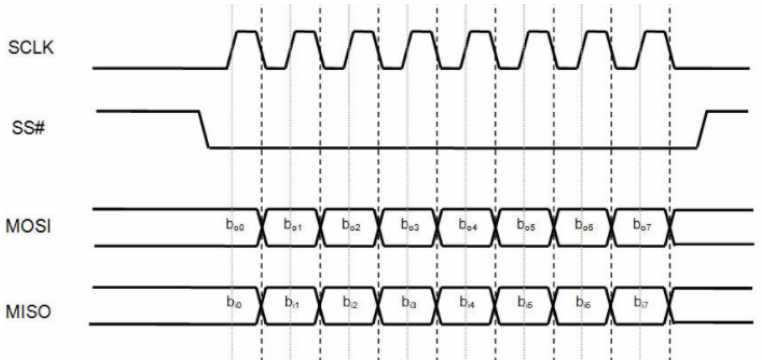

Figure 4.1: A simple SPI communication. Data bits on MOSI and MISO toggle on the SCLK falling edge and are sampled on the SCLK rising edge. The SPI mode defines which SCLK edge is used for toggling data and which SCLK edge is used for sampling data. Source: An introducction to I^2C and SPI Protocols by *Frédéric Leens*.

Physically, the bus consists on two-directional wires (SDA and SCL). The master is defined as the first device initiating the data transfer, relegating the rest to slaves. The data transfer starts by issuinf the start condition from the master. As this signal is received by the slaves, they start to listen for the next incoming signal, which consists on the address associated with the slave with which the master wants to start the communication together with the bit which indicates if it is a *write* or *read* operation. All the slaves that does not match the address on the signal with their own address will stop listening and will wait until the end of the communication, while the slave matching will send an acknowledgement signal to the master. Once the master receives the slave acknowledgement signal, the communication starts. When the communication ends, the master will send the stop condition to all slaves. This communication is 8-bit long and must wait until acknowledgement signal from the listening part; after this signal, emitter could send another 8-bit data or 1-bit to end the communication.

START	Slave address	Rd/nWr	ACK	Data	ACK	Data	ACK	STOP
1 bit	7 bits	1 bit	1 bit	8 bits	1 bit	8 bits	1 bit	1 bit

Figure 4.2: I^2C Data protocol sending 2 byte information in one sequence.

4.2.3. Analogic to Digital Converter

The sun sensor gives the output as analogical voltage. To make this data readable and let the OBC to operate with this data, an Analogic o Digital Converter (ADC) is needed. As the selected OBC (*ATmega382*) has integrated 6 ADC ports and the sun sensor (*nanoSSOC-A60*) has 4 analogic outputs, the own OBC will be used to convert the data.

ADC from OBC is 10-bit, taking into account that the sun sensor output voltage varies from 1 to 3.3V and has a field of view of $\pm$ 60°, the maximum resolution given by the ADC is:

$$\text{Resolution} = \frac{60-(-60)}{2^{10}} = 0.117^\circ$$

As the accuracy for the sensor itself is 0.5°, the ADC will not introduce an extra error on

the sensor readings.

It must be taken into account that the OBC needs individual supply for ADC at pin 20 and needs a reference voltage on pin 21. Reference voltage is defined as the maximum value which ADC can covert. In this case, as the output for the sun sensor is also 3.3V, pin 20 and pin 21 can be connected together in parallel with the main supply (pin 7).

4.3. Output signals

Once the data is received and processed on the OBC, it must distribute pertinent information packages to the RCDs in order to maintain on the correct attitude. Also, it is necessary to transmit the data to the transceiver to send all the data packages, as was seen on chapter 3. Finally, OBC must decide the logic outputs for the battery protection switches (s_1, s_2 and s_3) introduced on EPS (chapter 2).

4.3.1. RCDs

RCDs are attitude control devices which change their optical proprieties as a function of the voltage polarity, thus changing the centre of pressures and therefore the solar sail orientation. When voltage is +1 V, the surface bleaches increasing the reflectivity and gaining pressure on the RCD. Otherwise, when the voltage on the load is -1 V, the surface of the RCD gets coloured by increasing the absorptivity and reducing reflectivity, so reducing the solar pressure.

The function of OBC is to change the polarity of the voltage as a function of the inputs from the ADCS' sensors. For this purpose, an inverter bridge configuration will be used with a set of transistors attached to single bit output from the OBC. This inverter bridge consists of four transistors acting like electrical switches that close or open as a function of input bit.

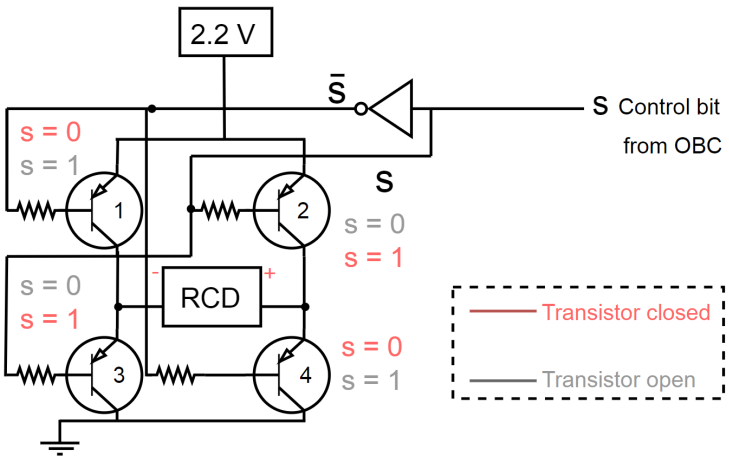

Figure 4.3: Inverter bridge which changes the polarity of the voltage in function of the bit "s" from the OBC.

It can be seen in figure 4.3 that when OBC sends s=1, the transistors 2 and 3 will be activated (closed). Meanwhile, the inverted signal from the OBC $\bar{s}$=0 lets the transistors 1 and 4 open. This leaves into a negative circulation (negative to positive pole of the RCD). In other words, the applied voltage is -1 V.

Then, when the pin associated with the control bit s is 1, the applied voltage to the load will be -1 V and the RCD will become less refelective, while when s is 0 the voltage on the load will be +1 V bleaching the surface and making it more reflective. As there exist 4 RCDs, one in each corner, it will be needed one control bit per each RCD with the subsequent inverter bridge.

The power source at 2.2V is due to the presence of the transistors. Both for s = 1 or s = 0, two transistors are in series with the RCD. Typical transistors have voltage drop of 0.6V; then, by letting 1 V to the RCD, the total voltage is 1 V + 2 $\times$ 0.6 V = 2.2 V.

4.3.2. Transceiver

Pins 2 and 3 in ATmega328 are designed for receiving and transmitting signals (respectively) by means of a serial interface USART (Universal Synchronous and Asynchronous Receiver-Transmitter). As the solar sail will only send information, and not receive any type of signal, only Tx pin (2) will be used. By transmitting all the data to the transceiver it will modulate to VSWR (Voltage standing wave ratio) and radiate the electromagnetic waves by using the patch antenna designed on chapter 3.

4.3.3. Battery protection switches

On EPS section (chapter 2) has been introduced the switches S_1, S_2 and S_3 that have the function of battery protection to avoid the possibility of over-charging by opening the fed connection.

Those switches are closed or open with digital outputs from the OBC, which decides to open or close circuit in response to the battery capacity read from analogical input (pin 11) and the internal clock. The logical scheme is:

- Internal clock value = n $\times$ 60(+2) minutes $\rightarrow S_1 = 0; S_2 = 0; S_3 = 1$ (burst state).
- Voltage on cell = full $\longrightarrow S_1 = 1; S_2 = 0; S_3 = 0$ (standby state).
- Voltage on cell != full $\longrightarrow S_1 = 1; S_2 = 1; S_3 = 0$ (regular state).

where 0 is open and 1 closed circuit. Burst state repeats periodically every 60 minutes and rest on this state for 2 minutes. If internal clock is not a multiple of an hour, the state could only be standby or regular. As a definition (see distribution chapter) standby only occurs when battery cell voltage is full. Then, if pin 11 reads full voltage system is on standby, otherwise it is on regular state.

4.4. Connection

ATmega328 has 28 pins. 20 of them are I/O ports, 14 of those ports are digital I/O, of which 6 have the possibility to give PWM outputs. The resting 6 ports are for analog I/O. Those leaves 8 ”special” pins, two of those pins are reserved for a crystal oscillator but, it can be used as digital I/O ports if internal clock is used. Another 2 pins are used just to power supply and ground. For the analog I/O ADC are needed another 3 ports, one for power supply, other for ground and other as voltage reference (referring to the maximum input from the analogical inputs). Finally, last bit is used as reset, allowing the program to re-start.

Pin	Function	Pin	Function	Pin	Function	Pin	Function
1	Reset	8	Ground	15	Digital pin *	22	Ground ADC
2	Digital (Rx)	9	Crystal osc	16	Digital pin *	23	Analog pin
3	Digital (Tx)	10	Crystal osc	17	Digital pin *	24	Analog pin
4	Digital pin	11	Digital pin *	18	Digital pin	25	Analog pin
5	Digital pin *	12	Digital pin *	19	Digital pin	26	Analog pin
6	Digital pin	13	Digital pin	20	Power ADC	27	Analog pin
7	Power	14	Digital pin	21	Reference voltage	28	Analog pin

Table 4.2: *ATmega328* pin description. Digital pins marked with * means that PWM output is enabled.

By summarizing all those information, the full OBC scheme is:

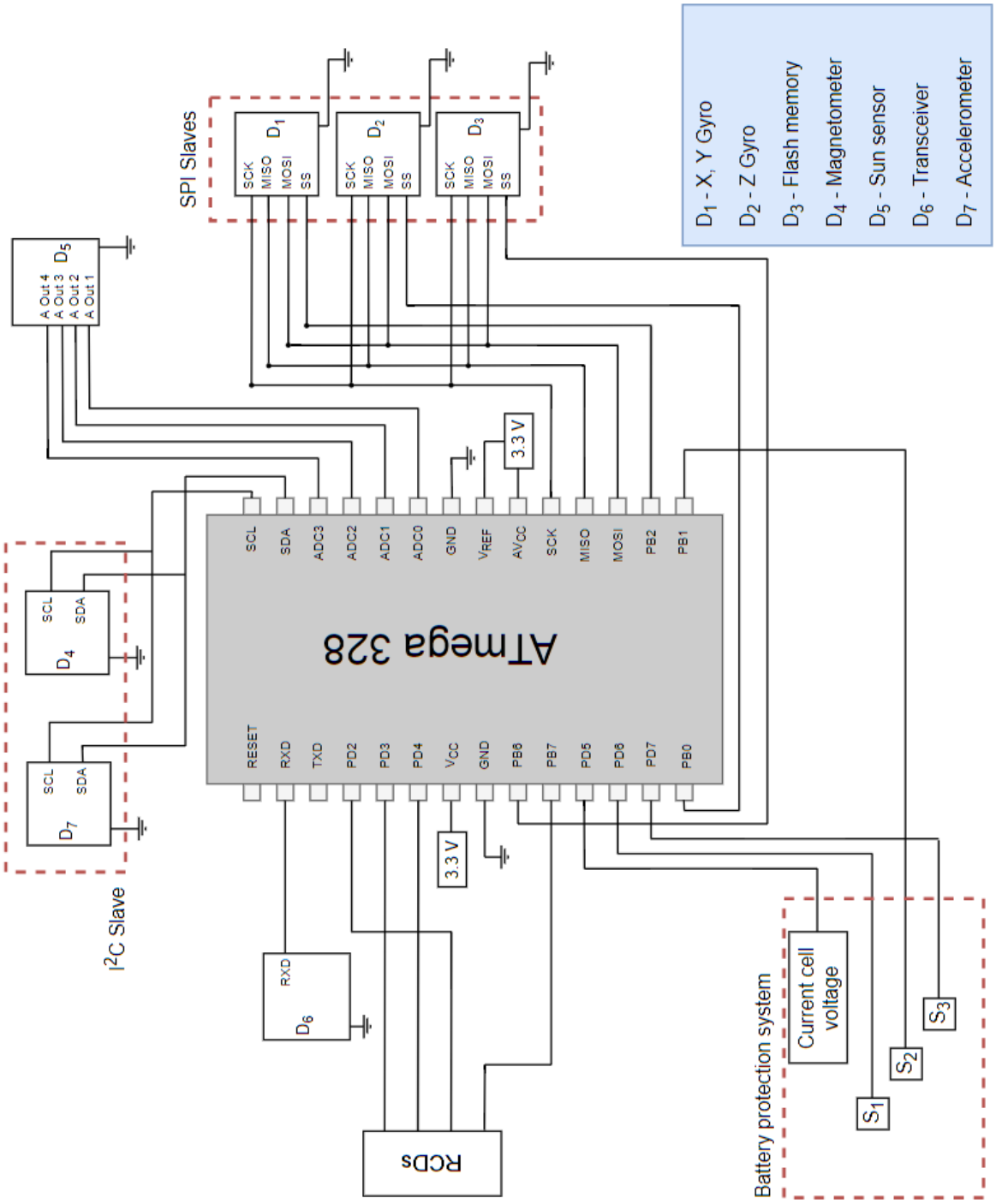

Figure 4.4: OBC Schematic.

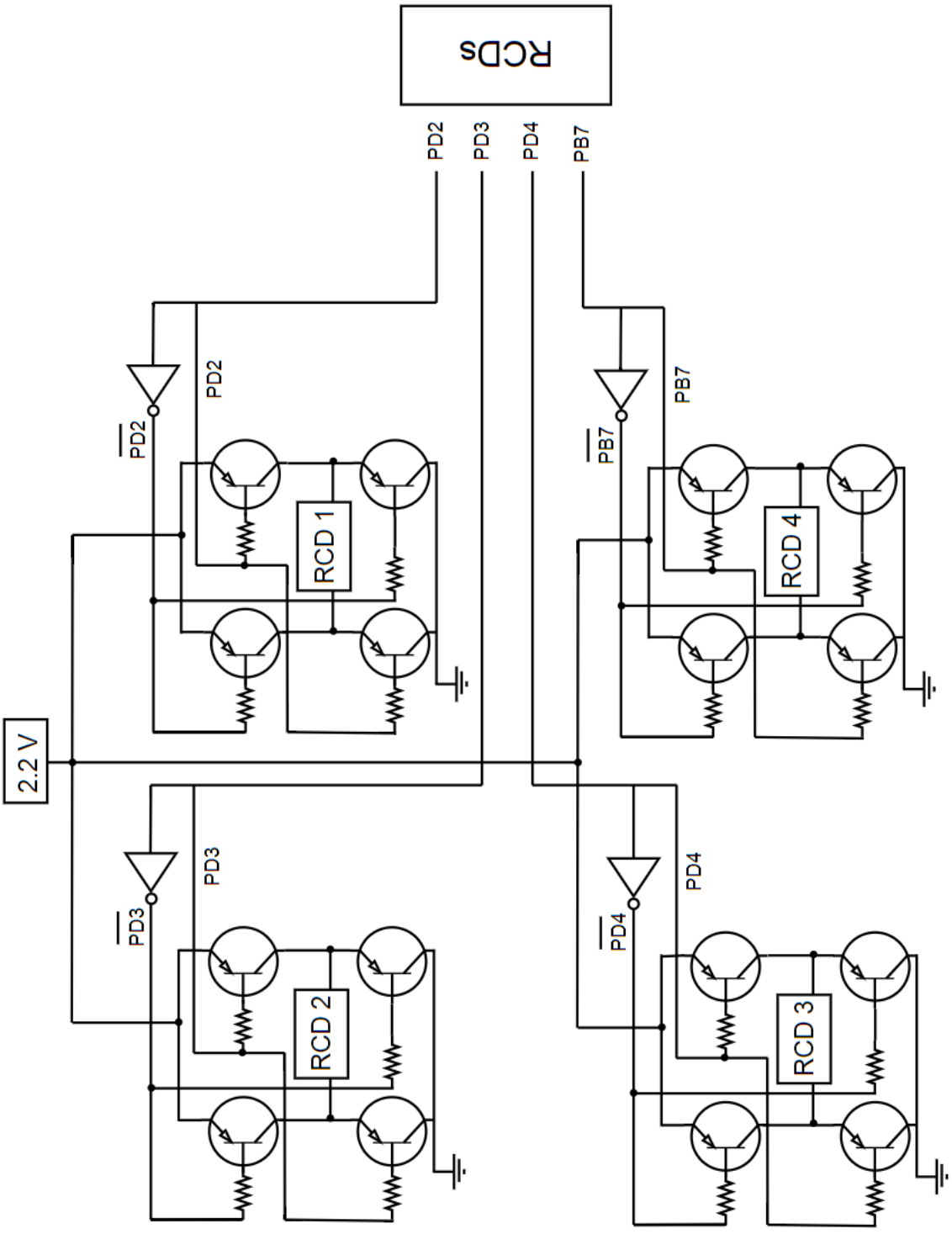
RCDs
PD2
PD3
PD4
PB7
2.2 V
PD2
PD2
RCD 1
PB7
PB7
RCD 4
PD3
PD3
RCD 2
PD4
PD4
RCD 3

CONCLUSIONS

As it was discussed on the introduction, the main problem along this project was the difficulty on reduce physically all the subsystems by keeping a high efficiency of the system in order to fulfil the mass requirements. Even with that, the requirement has been fulfilled with extra margin of 7 grams. All the devices with his sizes and masses involved on the all the sub-systems treated in this project are listed on the following table:

Device	**Model**	**Size (mm)**			**Weight (gr)**
Solar cell	Spectrolab 30.7	69.1	39.7	0.23	2.268
First stage booster	TPS61201	3.15	3.15	0.80	0.028
Bat. charge regulator	RP601x	1.95	1.95	0.64	0.020
Bat. output adapter	Polulu S78F3	17.78	12.70	2.54	5.670
Voltage step down	TPS6222x	3.05	3.05	1.10	0.006
Battery	SANYO 14500	49.1		13.85 ⊘	20.00
Battery coating	Aluminized kapton				0.077
OBC	ATmega328	37.4	6.76	3.28	3.700
External Flash	AT25DF512C	6.40	3.00	1.20	0.540
16x Transistor	610-2N3904	4.32	4.45	3.30	0.005
Magnetometer	LIS3MDL	2.00	2.00	1	0.018
Transceiver	INST 11b	5.00		20.0 ⊘	2.000
Antenna	Custom	1.60		37.2 ⊘	8.500
Total weight					**42.832**

Concerning about EPS, one of the most critical devices was the search of a battery, the discard of conventional space qualified batteries for being too heavy and the capacitors for being unable to provide energy for relatively long time periods leaves as only possibility the use of commercial batteries. Fortunately, other missions like *UNISAT-2* have been used this type of solution as experiment with satisfactory results. Even with it, it is assumed the intrinsic risk of using non-space qualified batteries as main (and unique) power storage. On the other hand, it is considered that the risk is low enough and that can not be achieved the requirements without take any risk.

Other critical point on the project was the search of the antenna, because of the very specific conditions to which it had to operate it have been necessary to investigate about the theory on micro-strip antenna in order to design custom circular patch antenna to fulfil all the requirements. The final theoretical results have been tested by using the software *ANSYS HFSS* to simulate the behaviour of it. Obtaining really positive results by accomplishing the difficult task of transmit information at huge distances up to 259 R_E with low transmitter power and low gain antenna.

By the OBC, they where not found problems to fulfil the mass requirement since microprocessors have been optimized to the maximum along the last years, the difficulty on this chapter has only attached to the technical difficulties on the understanding communication protocols and the architecture of microcontrollers and understand the difference

between memory types in order to select the most suitable one to store the data before the communication burst.

Finally, it can be said that the design of the bus for a very small solar sail have been fulfilled, accomplishing the objectives mentioned on the introduction where it was said that the electronic must fulfil all the necessary tasks to support the payload, as well as the ADCS system with only 50 grams.

In the development of this project it has not been studied deeply all the possibilities due to the impossibility in terms of time and knowledge. One of the aspects which could be of greater interest on future works could to study the possibility of use those 7 extra grams adding other sensors as payload to collect more information about the environment near L2, taking into account the overcharge this would mean to the communication subsystem, OBC and, subsequently, EPS.

BIBLIOGRAPHY

[1] Macdonald, M. (Ed.). (2014). *Advances in solar sailing*. Springer Science & Business Media.

[2] Larson, W. J., & Wertz, J. R. (1992). *Space mission analysis and design* (No. DOE/NE/32145–T1). Microcosm, Inc., Torrance, CA (US).

[3] Tsurutani, B. T., & Rosenvinge, T. T. (1984). ISEE-3 distant Geotail results. Geophysical Research Letters, 11(10), 1027-1029.

[4] Slavin, J. A., Smith, E. J., Tsurutani, B. T., Sibeck, D. G., Singer, H. J., Baker, D. N., ... & Scarf, F. L. (1984). Substorm associated traveling compression regions in the distant tail: ISEE-3 Geotail observations. Geophysical research letters, 11(7), 657-660.

[5] Juhan Frank (2006). *PHYS 7221 - The Three-Body Problem*

[6] Broucke, R., & Lass, H. (1973). A note on relative motion in the general three-body problem. Celestial Mechanics and Dynamical Astronomy, 8(1), 5-10.

[7] Ness, N. F. (1969). *The geomagnetic tail. Reviews of Geophysics*, 7(1-2), 97-127.

[8] Beech, W. A., Nielsen, D. E., Noo, J. T., & Ncuu, L. K. (1997). *AX. 25 Link Access Protocol for Amateur Packet Radio*, Version: 2.2 Rev. In Tucson Amateur Packet Radio Corp.

[9] KWAHA, B. J.; INYANG, O. N.; AMALU, P. *The circular microstrip patch antenna–design and implementation*. IJRRAS, 2011, vol. 8, no 1.

[10] Gupta, K., Jain, K., & Singh, P. (2014). *Analysis and design of circular microstrip patch antenna at 5.8 GHz*. IJCSIT) International Journal of Computer Science and Information Technologies.

[11] Shaw, J. A. (2013). *Radiometry and the Friis transmission equation*. American journal of physics, 81(1), 33-37.

[12] Anspaugh, B. E. (1996). *GaAs solar cell radiation handbook*.

[13] Green, M. A. (2006). Third generation photovoltaics. New York: Springer.

[14] AZ technology (2008). *Spacecraft Thermal Control and Conductive Paints/Coatings and Services Catalog.*

[15] Green, M. A., & Emery, K. (1993). *Solar cell efficiency tables*. Progress in Photovoltaics: Research and Applications, 1(1), 25-29.

[16] Varshni, Y. P. (1967). Temperature dependence of the energy gap in semiconductors. physica, 34(1), 149-154.

[17] Rappaport, P. (1959). *The photovoltaic effect and its utilization*. Solar Energy, 3(4), 8-18.

[18] Barnhart, D. J., Vladimirova, T., & Sweeting, M. N. (2007). *Very small satellite design for distributed space missions*. Journal of Spacecraft and Rockets, 44(6), 1294-1306.

[19] Santoni, F., Tortora, P., Alessandrini, F., & Passerini, S. (2002, May). *Commercial Li Ion Batteries for Nanosatellite Applications Flight Experiment*. In Space Power (Vol. 502, p. 653).

[20] Leens, F. (2009). *An introduction to I 2 C and SPI protocols*. IEEE Instrumentation & Measurement Magazine, 12(1), 8-13.

[21] Jordi L. Gutiérrez. *Power Subsystem* [PowerPoint slides].

[22] Jordi L. Gutiérrez. *Communication Subsystem* [PowerPoint slides].

[23] Jordi L. Gutiérrez. *On board computer* [PowerPoint slides].

Datasheet links:

Spectrolab solar cell	http://www.spectrolab.com/DataSheets/cells/XTJ_Prime_Data_Sheet_7-28-2016.pdf
AzurSpace solar cell	http://www.azurspace.com/images/0003429-01-01_DB_3G30C-Advanced.pdf
SolAero solar cell	http://solaerotech.com/wp-content/uploads/2016/10/ZTJ-Datasheet-Updated-2016.pdf
First stage voltage booster ..	http://www.ti.com/lit/ds/symlink/tps61200.pdf
Baterry charge regulator	http://www.mouser.com/ds/2/792/rp601-e-962707.pdf
Battery output adapter	https://www.tme.eu/es/Document/b624253546ed4f0eaaa2b862bcbefa9e/POLOLU-2122.pdf
Voltage step down	http://www.ti.com/lit/ds/symlink/tps62220.pdf
Battery	https://www.tme.eu/es/Document/89dd0fe7f9fb7fc9d798f4551238a5a8/ACCU-14500-0.8S.pdf
Magnetometer	http://www.st.com/content/ccc/resource/technical/document/datasheet/54/2a/85/76/e3/97/42/18/DM00075867.pdf/files/DM00075867.pdf/jcr:content/translations/en.DM00075867.pdf
ATmega328	http://www.atmel.com/Images/Atmel-42735-8-bit-AVR-Microcontroller-ATmega328-328P_Datasheet.pdf
External Flash	http://www.mouser.com/ds/2/590/DS-AT25DF512C_030-1153950.pdf
X, Y Gyro	http://site.eet-china.com/arrow/technote/ADI/ADXRS290.pdf
Z Gyro	http://www.analog.com/media/en/technical-documentation/data-sheets/ADXRS453.pdf
Accelerometer	http://www.mouser.com/ds/2/389/iis2dh-954784.pdf
Sun sensor	https://www.cubesatshop.com/wp-content/uploads/2016/06/nanoSSOC-A60-Brochure-1.pdf

APPENDICES

APPENDIX A. SPECTROLAB 30.7% XTJ PRIME

60th Anniversary!

XTJ PRIME

SPECTROLAB

A BOEING COMPANY

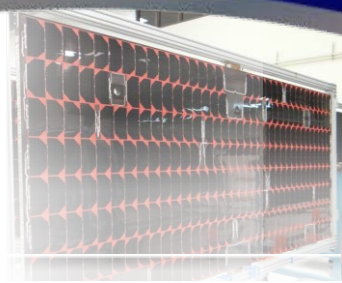

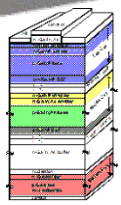

30.7% Triple Junction Space Grade Solar Cell

- Currently in full production
- Best In class - BOL & EOL
- AIAA-S111 & AIAA-S112 Qualified
- Heritage Upright Latice Matched XTJ Structure
- 26.7% EOL, 1E15 1MeV electron**
- Multiple sizes avilable (27cm² through 84 cm²)

Cell Thickness **= 80 µm - 225 µm**

Cell Mass = 50 – 84mg/cm²

XTJ Prime (US Standard- AIAA-S111-2005)

Parameters*	BOL	5E14	1E15	3E15	1E16
$Efficiency_{mp}$	30.7%	.88	.85	.76	.65
V_{OC} (V)	2.715	.89	.87	.83	.78
J_{sc} (mA/cm²)	18.1	.99	.98	.96	.93
V_{mp} (V)	2.390	.89	.87	.83	.76
J_{mp} (mA/cm²)	17.4	.99	.97	.92	.86

**Production Average; AM0 (135.3 mW/cm²) 28°C*

(Fluence 1MeV Electrons/cm²)

XTJ Prime (European Standard - ECSS**)

Parameters*	BOL	5E14	1E15	3E15	1E16
$Efficiency_{mp}$	30.7%	.90	.87	.80	.70
V_{OC} (V)	2.715	.90	.88	.85	.80
J_{sc} (mA/cm²)	18.1	.99	.99	.97	.94
V_{mp} (V)	2.390	.91	.89	.85	.80
J_{mp} (mA/cm²)	17.4	.99	.98	.94	.88

*** Photon and temperature annealing according to ECSS-E-ST-20-08C*

ENVIRONMENTAL MANAGEMENT SYSTEM
CERTIFIED BY DNV
ISO 14001

AS9100 REGISTERED

ISO 9001 2008

Spectrolab, Inc. 12500 Gladstone Avenue, Sylmar, California 91342 USA
● Phone: 818.365.4611 ● FAX: 818.361.5102 ● Website: www.spectrolab.com

60th Anniversary!

XTJ PRIME

SPECTROLAB

A BOEING COMPANY

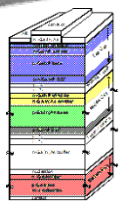

30.7% Triple Junction Space Grade Solar Cell

Temperature Coefficients (15°C - 75°C)

Parameters	5E14	1E15	3E15	1E16
$\Delta V_{oc}/\Delta T$ (mV/C°)	-6.2	-6.3	-6.5	-6.6
$\Delta J_{sc}/\Delta T$ (uA/cm^2/C°)	10	11	11	12
$\Delta V_{mp}/\Delta T$ (mV/C°)	-6.5	-6.6	-6.7	-6.7
$\Delta J_{mp}/\Delta T$ (uA/cm^2/C°)	8.9	10.3	12	12

Thermal Parameters	Value
Solar Absorptance	0.88
Emittance	0.85

Operates 2° C Cooler Than Other Space Grade Solar Cells

Standard Cell Sizes

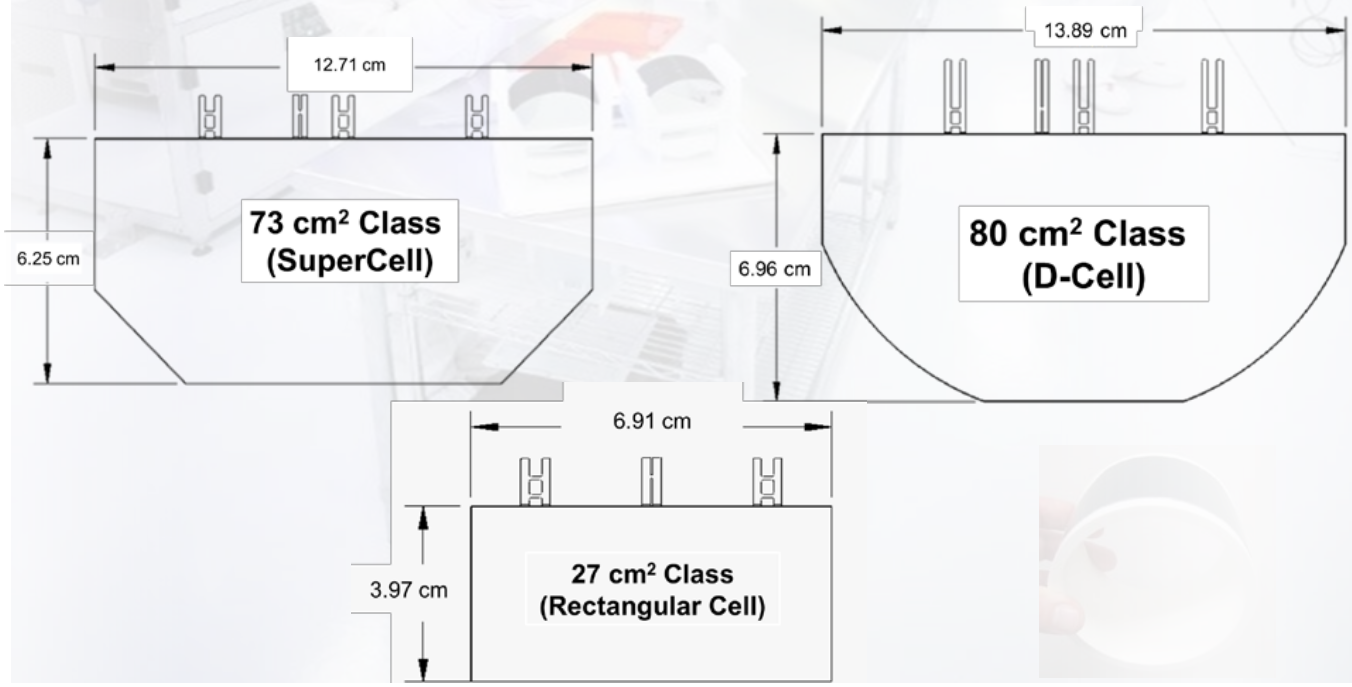

Spectrolab, Inc. 12500 Gladstone Avenue, Sylmar, California 91342 USA
• Phone: 818.365.4611 • FAX: 818.361.5102 • Website: www.spectrolab.com

APPENDIX B. AZURSPACE 30% 3G30C

AZURSPACE
SOLAR POWER GMBH

30% Triple Junction GaAs Solar Cell

Type: TJ Solar Cell 3G30C - Advanced

Best in Class EOL-Values!

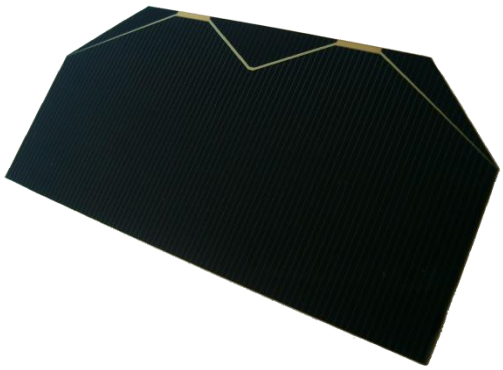

This cell type is a GaInP/GaAs/Ge on Ge substrate triple junction solar cell (efficiency class 30% advanced). The end-of-life version of the 3G30C solar cell offers best EOL-performance values and should be combined with an external bypass diode protection.

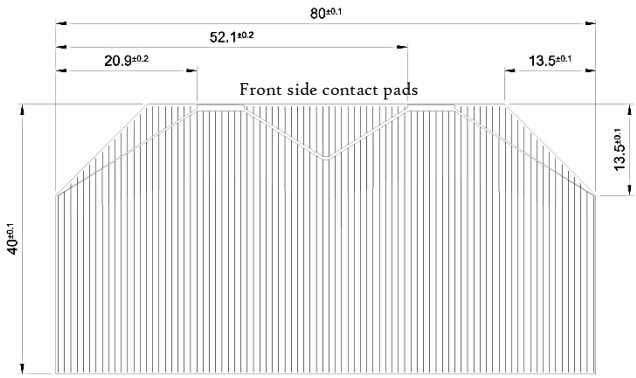

3G30C - Advanced

Space

30% Triple Junction GaAs Junction Solar Cell
Type: TJ Solar Cell 3G30C - Advanced

Design and Mechanical Data

Base Material	GaInP/GaAs/Ge on Ge substrate
AR-coating	TiO_x/Al_2O_3
Dimensions	40 x 80 mm ± 0.1 mm
Cell Area	30.18 cm^2
Average Weight	≤ 86 mg/cm^2
Thickness (without contacts)	150 ± 20 µm
Contact Metallization Thickness (Ag/Au)	4 – 10 µm
Grid Design	Grid system with 2 contact pads

Electrical Data

		BOL	2,5E14	5E14	1E15
Average Open Circuit V_{oc}	[mV]	2700	2616	2564	2522
Average Short Circuit I_{sc}	[mA]	520.2	518.5	514.0	501.9
Voltage at max. Power V_{mp}	[mV]	2411	2345	2290	2246
Current at max. Power I_{mp}	[mA]	504.4	503.2	500.6	486.6
Average Efficiency η_{bare} (1367 W/m^2)	[%]	29.5	28.6	27.8	26.5
Average Efficiency η_{bare} (1353 W/m^2)	[%]	29.8	28.9	28.1	26.8

Standard: CASOLBA 2005 (05-20MV1, etc); Spectrum: AMO WRC = 1367 W/m^2; T = 28 °C @fluence 1MeV [e/cm^2]

Acceptance Values

Voltage V_{op}	2350 mV
Min. average current $I_{op\ avg}$ @ V_{op}	505 mA
Min. individual current $I_{op\ min}$ @ V_{op}	475 mA

Temperature Gradients

			BOL	2,5E14	5E14	1E15
Open Circuit Voltage	$\Delta V_{oc}/\Delta T\uparrow$	[mV/°C]	- 6.2	- 6.5	- 6.6	- 6.7
Short Circuit Current	$\Delta I_{sc}/\Delta T\uparrow$	[mA/°C]	0.36	0.33	0.35	0.38
Voltage at max. Power	$\Delta V_{mp}/\Delta T\uparrow$	[mV/°C]	- 6.7	- 6.8	- 7.1	- 7.2
Current at max. Power	$\Delta I_{mp}/\Delta T\uparrow$	[mA/°C]	0.24	0.20	0.24	0.28

@fluence 1MeV [e/cm^2]

Threshold Values

Absorptivity	≤ 0.91 (with CMX 100 AR)
Pull Test	> 1.6 N at 45° welding test (with 12.5µm Ag stripes)
Status	Qualified

3G30C - Advanced

AZUR SPACE Solar Power GmbH
Theresienstr. 2
74072 Heilbronn
phone: +49 7131 67 2603
telefax: +49 7131 67 2727
e-mail: info@azurspace.com
website: www.azurspace.com

Certified Company

ISO 9001
ISO 14001
OHSAS 18001

Space

APPENDIX C. SOLAERO 29.5% ZTJ

AZURSPACE
SOLAR POWER GMBH

30% Triple Junction GaAs Solar Cell

Type: TJ Solar Cell 3G30C - Advanced

Best in Class EOL-Values!

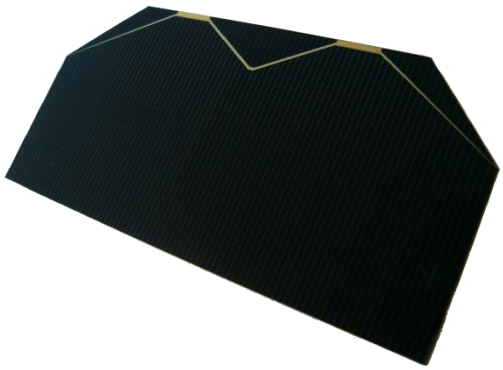

This cell type is a GaInP/GaAs/Ge on Ge substrate triple junction solar cell (efficiency class 30% advanced). The end-of-life version of the 3G30C solar cell offers best EOL-performance values and should be combined with an external bypass diode protection.

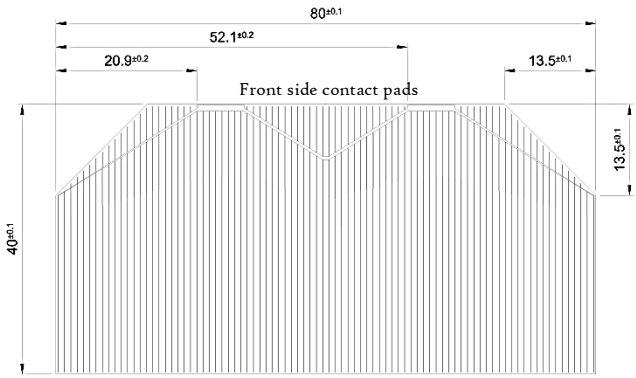

3G30C - Advanced

Space

30% Triple Junction GaAs Junction Solar Cell
Type: TJ Solar Cell 3G30C - Advanced

Design and Mechanical Data

Base Material	GaInP/GaAs/Ge on Ge substrate
AR-coating	TiO_x/Al_2O_3
Dimensions	40 x 80 mm ± 0.1 mm
Cell Area	30.18 cm^2
Average Weight	≤ 86 mg/cm^2
Thickness (without contacts)	150 ± 20 µm
Contact Metallization Thickness (Ag/Au)	4 – 10 µm
Grid Design	Grid system with 2 contact pads

Electrical Data

		BOL	2,5E14	5E14	1E15
Average Open Circuit V_{oc}	[mV]	2700	2616	2564	2522
Average Short Circuit I_{sc}	[mA]	520.2	518.5	514.0	501.9
Voltage at max. Power V_{mp}	[mV]	2411	2345	2290	2246
Current at max. Power I_{mp}	[mA]	504.4	503.2	500.6	486.6
Average Efficiency η_{bare} (1367 W/m^2)	[%]	29.5	28.6	27.8	26.5
Average Efficiency η_{bare} (1353 W/m^2)	[%]	29.8	28.9	28.1	26.8

Standard: CASOLBA 2005 (05-20MV1, etc); Spectrum: AMO WRC = 1367 W/m^2; T = 28 °C @fluence 1MeV [e/cm^2]

Acceptance Values

Voltage V_{op}	2350 mV
Min. average current $I_{op\ avg}$ @ V_{op}	505 mA
Min. individual current $I_{op\ min}$ @ V_{op}	475 mA

Temperature Gradients

			BOL	2,5E14	5E14	1E15
Open Circuit Voltage	$\Delta V_{oc}/\Delta T\uparrow$	[mV/°C]	- 6.2	- 6.5	- 6.6	- 6.7
Short Circuit Current	$\Delta I_{sc}/\Delta T\uparrow$	[mA/°C]	0.36	0.33	0.35	0.38
Voltage at max. Power	$\Delta V_{mp}/\Delta T\uparrow$	[mV/°C]	- 6.7	- 6.8	- 7.1	- 7.2
Current at max. Power	$\Delta I_{mp}/\Delta T\uparrow$	[mA/°C]	0.24	0.20	0.24	0.28

@fluence 1MeV [e/cm^2]

Threshold Values

Absorptivity	≤ 0.91 (with CMX 100 AR)
Pull Test	> 1.6 N at 45° welding test (with 12.5µm Ag stripes)
Status	Qualified

3G30C - Advanced

AZUR SPACE Solar Power GmbH
Theresienstr. 2
74072 Heilbronn
phone: +49 7131 67 2603
telefax: +49 7131 67 2727
e-mail: info@azurspace.com
website: www.azurspace.com

Certified Company

ISO 9001
ISO 14001
OHSAS 18001

Space

APPENDIX D. QIOPTIC SOLAR CELL COVERGLASSES

QIOPTIQ
Photonics for Innovation
An Excelitas Technologies Company

Solar Cell Coverglasses

Designed and manufactured to provide radiation protection

Qioptiq

- Design and manufacture of radiation-stable Coverglasses
- Over 40 years of Space Heritage
- Space Qualified
- Choice of glass types (CMX, CMG, CMO)
- Worlds leading manufacturer
- Bespoke solutions

Minimum Coverglass Transmission specifications with 0.10mm thick CMX, CMG and CMO glass types

		350 - 400nm	400 - 450nm	450 - 700nm	600 - 800nm	650 - 900nm	450 - 1100nm	900 - 1800nm	IR Cut-off	Min Emittance	Front Surface Resistance
CMX	Uncoated	73.5	91.5	94.0	95.0	95.0	95.0	95.0		0.88	
CMG		83.5	92.5	94.5	95.0	95.0	95.0	95.0		0.88	
CMO		88.0	94.0	94.5	95.0	95.0	95.0	95.0		0.88	
CMX	AR	73.5	93.0	96.5	97.5	97.5	96.5	96.5		0.88	
CMG		83.5	94.0	97.0	97.5	97.5	96.5	96.5		0.88	
CMO		88.0	95.5	97.0	97.5	97.5	96.5	96.5		0.88	
CMX	Conductive	73.5	94.0	96.5	97.0	97.0	96.5	96.0		0.86	<10M Ohms
CMG	AR	83.5	95.0	97.0	97.0	97.0	96.5	96.0		0.86	<10M Ohms
CMO		88.0	96.0	97.0	97.0	97.0	96.5	96.0		0.86	<10M Ohms
CMX	Conductive	71.0	89.0	94.0	95.0	95.0	94.5	94.5		0.84	<5K Ohms
CMG		80.0	89.0	94.0	95.0	95.0	94.5	94.5		0.84	<5K Ohms
CMO		80.0	89.0	94.0	95.0	95.0	94.5	94.5		0.84	<5K Ohms
CMX	UV Reflector	73.5	92.0	96.0	96.5	96.5	96.0	94.0		0.86	
CMG		83.5	93.0	96.5	96.5	96.5	96.0	94.0		0.86	
CMO		88.0	94.5	96.5	96.5	96.5	96.0	94.0		0.86	
CMX	AR/IRR Silicon	73.5	89.0	96.0	96.0	96.0	95.0		1165+/-	0.86	
CMG	Blue Red Silicon	83.5	90.0	96.0	96.0	96.0	95.0		50nm	0.86	
CMO		88.0	92.0	96.0	96.0	96.0	95.0			0.86	
CMX	UVR/IRR	73.5	92.0	96.5	96.5	96.5	95.0		1315+/-	0.86	
CMG	Triple Junction	83.5	93.0	96.5	96.5	96.5	95.0		35nm	0.86	
CMO	(PS 703)	88.0	88.0	96.5	96.5	96.5	95.0			0.86	

1. All spectral data measured at normal incidence in 1.43 matching index
2. Tolerances on specification values are available from relevant product specifications
3. Spectral data is for 0.10mm/0.004" coverglasses, please refer to relevant specification for spectral performance of other thicknesses.

Mechanical Properties

Thickness:	0.050mm to 0.50mm / 0.002" to 0.02" Special thicknesses on request
Tolerancing:	LxW ± 0.05mm / 0.002"
Surface Finish:	As drawn to: MIL-PRF-13830B, 80/50 scratch dig
Parallelism:	0.05mm per 20mm
Perpendicularity:	90° ± 0° 30'
Coating:	Uncoated area, masked by coating tooling, shall not exceed 1% of the total coverglass area
Edge Quality:	Chemically etched for strength enhancement
Toughening:	CMX and CMG glass can be chemically toughened if required
Humidity Resistance:	98% ± 2% relative humidity for 72 hours @ 50°C ± 20°C
Adhesion:	Using cellulose tape to MIL-M-13508
Abrasion:	20 strokes with 6mm pencil type eraser to MIL-E-12397 loaded to 10N
Radiation Resistance:	UV exposure, electron, low energy proton, high energy proton - please refer to relevant specifications
Thermal Cycling:	Details on request

Physical Properties

	CMX	CMG	CMO
Density:	2.60 ± 0.02g cm^3	2.54 ± 0.02g cm^3	2.54 ± 0.02g cm^3
Thermal Expansion Coefficient:			
Average over range -100˚C to 100˚C	6.0 ± 0.75 x 10^{-6}/˚C	5.5 ± 0.75 x 10^{-6}/˚C	5.5 ± 0.75 x 10^{-6}/˚C
Average over range -100˚C to 200˚C	6.5 ± 0.75 x 10^{-6}/˚C	6.0 ± 0.75 x 10^{-6}/˚C	6.0 ± 0.75 x 10^{-6}/˚C
Average over range +30˚C to 200˚C	7.0 ± 0.75 x 10^{-6}/˚C	6.5 ± 0.75 x 10^{-6}/˚C	6.5 ± 0.75 x 10^{-6}/˚C
Youngs Modulus:	75.0 ± 2 GNm^{-2}	77.0 ± 2 GNm^{-2}	70 ± 2 GNm^{-2}
Poissons Ratio:	0.21 ± 0.05	0.20 ± 0.05	0.22 ± 0.05
Bulk Resistivity:			
At 20˚C	11.5 ± 1 log ohm meter	13.5 ± 1 log ohm meter	16.0 ± 1 log ohm meter
At 60˚C	10.0 ± 1 log ohm meter	11.5 ± 1 log ohm meter	14.0 ± 1 log ohm meter
Refractive Index:	1.524 – 1.530	1.513 – 1.519	1.510 – 1.516

For technical information contact:

sales@uk.qioptiq.com
phone +44 (0)1745 589833
www.qioptiq.com

APPENDIX E. LIS3MDL

LIS3MDL

Digital output magnetic sensor: ultra-low-power, high-performance 3-axis magnetometer

Datasheet - production data

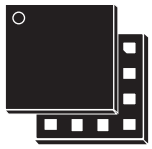

LGA-12 (2.0x2.0x1.0 mm)

Features

- Wide supply voltage, 1.9 V to 3.6 V
- Independent IO supply (1.8 V)
- ±4/±8/±12/±16 gauss selectable magnetic full scales
- Continuous and single-conversion modes
- 16-bit data output
- Interrupt generator
- Self-test
- I^2C/SPI digital output interface
- Power-down mode / low-power mode
- ECOPACK®, RoHS and “Green” compliant

Applications

- Magnetometers
- Compasses

Description

The LIS3MDL is an ultra-low-power high-performance three-axis magnetic sensor.

The LIS3MDL has user-selectable full scales of ±4/±8/±12/±16 gauss.

The self-test capability allows the user to check the functioning of the sensor in the final application.

The device may be configured to generate interrupt signals for magnetic field detection.

The LIS3MDL includes an I^2C serial bus interface that supports standard and fast mode (100 kHz and 400 kHz) and SPI serial standard interface.

The LIS3MDL is available in a small thin plastic land grid array package (LGA) and is guaranteed to operate over an extended temperature range of -40 °C to +85 °C.

Table 1. Device summary

Order codes	Temperature range [°C]	Package	Packaging
LIS3MDLTR	-40 to +85	LGA-12	Tape and reel